

# MIF Deficiency Reduces Chronic Inflammation in White Adipose Tissue and Impairs the Development of Insulin Resistance, Glucose Intolerance, and Associated Atherosclerotic Disease

Lars Verschuren, Teake Kooistra, Jürgen Bernhagen, Peter J. Voshol, D. Margriet Ouwers, Marjan van Erk, Jitske de Vries-van der Weij, Lin Leng, J. Hajo van Bockel, Ko Willems van Dijk, Günter Fingerle-Rowson, Rick Bucala, Robert Kleemann

**Abstract**—Chronic inflammation in white adipose tissue (WAT) is positively associated with obesity, insulin resistance (IR) and the development of type 2 diabetes. The proinflammatory cytokine MIF (macrophage migration inhibitory factor) is an essential, upstream component of the inflammatory cascade. This study examines whether MIF is required for the development of obesity, IR, glucose intolerance, and atherosclerosis in the LDL receptor-deficient ( $Ldlr^{-/-}$ ) mouse model of disease.  $Ldlr^{-/-}$  mice develop IR and glucose intolerance within 15 weeks, whereas  $Mif^{-/-}Ldlr^{-/-}$  littermates are protected. MIF deficiency does not affect obesity and lipid risk factors but specifically reduces inflammation in WAT and liver, as reflected by lower plasma serum amyloid A and fibrinogen levels at baseline and under inflammatory conditions. Conversely, MIF stimulates the in vivo expression of human C-reactive protein, an inflammation marker and risk factor of IR and cardiovascular disease. In WAT, MIF deficiency reduces nuclear c-Jun levels and improves insulin sensitivity; MIF deficiency also reduces macrophage accumulation in WAT and blunts the expression of two proteins that regulate macrophage infiltration (intercellular adhesion molecule-1, CD44). Mechanistic parallels to WAT were observed in aorta, where the absence of MIF reduces monocyte adhesion, macrophage lesion content, and atherosclerotic lesion size. These data highlight the physiological importance of chronic inflammation in development of IR and atherosclerosis and suggest that MIF is a potential therapeutic target for reducing the inflammatory component of metabolic and cardiovascular disorders. (*Circ Res.* 2009;105:99-107.)

**Key Words:** inflammation ■ cytokines ■ atherosclerosis ■ insulin resistance ■ C-reactive protein

The intertwined medical problems of obesity, glucose intolerance, type 2 diabetes (T2D), dyslipidemia, and atherosclerosis form the most serious threats to public health worldwide. Insulin resistance (IR) is an integral feature of the medical sequelae that are collectively referred to as the metabolic syndrome.<sup>1</sup> Decreased insulin sensitivity is the underlying defect in >90% of patients with T2D, and it is also considered to be a major pathological mechanism for the associated development of cardiovascular disease.<sup>2</sup>

Recent human and animal studies have established both correlative and causative links between IR and chronic inflammation, in particular within adipose tissue.<sup>3,4</sup> For example, C-reactive protein (CRP), which is a serum marker of systemic inflammation, is independently related to insulin insensitivity and highly predictive for progression to overt

T2D.<sup>5</sup> Mechanistic studies that have evaluated the impact of blocking specific inflammatory control points, such as c-Jun N-terminal kinase (JNK)1,<sup>6</sup> support the concept that the persistent activation of proinflammatory transcription factors (eg, c-Jun) in critical metabolic sites (adipose and liver tissue) may underlie the development of IR. When chronically inflamed, these tissues release proinflammatory molecules, including cytokines, acute-phase reactants, and procoagulant factors (eg, interleukin [IL]-6, serum amyloid A [SAA], CRP, fibrinogen), which can participate in the pathogenesis of IR and atherosclerosis.<sup>3,7-9</sup> A primary event in the pathogenesis of IR is the infiltration of macrophages into white adipose tissue (WAT). This process appears to be of critical importance for the development of low-grade adipose tissue inflammation, and it may be a unifying mechanism for the devel-

Original received October 3, 2008; resubmission received April 14, 2009; accepted May 20, 2009.

From the Gaubius Laboratory (L.V., T.K., J.d.V.-v.d.W., R.K.), TNO-Quality of Life, BioSciences, Leiden, The Netherlands; Departments of Vascular Surgery (L.V., J.H.v.B., R.K.), Molecular Cell Biology (D.M.O.), Endocrinology (P.J.V.), Human Genetics (J.d.V.-v.d.W., K.W.v.D.), and Internal Medicine (J.d.V.-v.d.W., K.W.v.D.), Leiden University Medical Center, The Netherlands; Department of Biochemistry and Molecular Cell Biology (J.B.), RWTH Aachen University, Germany; Physiological Genomics (M.v.E.), TNO-Quality of Life, BioSciences, Zeist, The Netherlands; Department of Hematology and Oncology (G.F.-R.), Clinic-I for Internal Medicine, University Hospital Cologne, Germany; and Department of Medicine and Pathology (L.L., R.B.), School of Medicine, Yale University, New Haven, Conn.

Correspondence to Robert Kleemann, PhD, TNO-BioSciences, Zernikedreef 9, 2301 CE Leiden, The Netherlands. E-mail Robert.Kleemann@tno.nl  
© 2009 American Heart Association, Inc.

*Circulation Research* is available at <http://circres.ahajournals.org>

DOI: 10.1161/CIRCRESAHA.109.199166

**Table. Effects of MIF Deficiency on Markers of Cardiovascular and Metabolic Disease**

	Twelve Weeks Old		Thirty-Five Weeks Old	
	Ldlr <sup>-/-</sup>	Mif <sup>-/-</sup> Ldlr <sup>-/-</sup>	Ldlr <sup>-/-</sup>	Mif <sup>-/-</sup> Ldlr <sup>-/-</sup>
Plasma cholesterol, mmol/L	5.6±1.0	5.7±1.3	11.4±1.7	14.0±3.3
Plasma triglyceride, mmol/L	1.7±0.4	1.6±0.3	2.6±0.7	2.9±1.3
Plasma free fatty acid, mmol/L	0.84±0.19	0.87±0.23	0.50±0.20	0.61±0.13
Food intake, g/d	5.4±0.5	5.0±0.7	4.6±0.3	4.9±0.3
Body weight (start), g	28.4±2.9	28.6±2.9	38.2±5.4	36.1±4.6 g
Plasma leptin, ng/mL	3.5±1.9	3.4±2.5	146.1±47.3	146.3±54.8
Plasma fibrinogen, mg/mL	2.4±0.8	1.8±0.5	4.7±0.8	3.0±0.4*
Plasma SAA, μg/mL	8.4±4.9	2.4±1.0*	109±14	10±7*

Male Ldlr<sup>-/-</sup> and Mif<sup>-/-</sup>Ldlr<sup>-/-</sup> mice were fed a chow diet and were monitored over time. Data are means±SD (n≥10 per genotype). \*P<0.05.

opment of IR and atherosclerosis.<sup>3</sup> Nevertheless, our understanding of the factors that contribute to WAT inflammation is incomplete, and from a therapeutic perspective, it remains unclear if inflammatory pathways can be manipulated for clinical benefit.

MIF (macrophage migration inhibitory factor) is a widely expressed proinflammatory cytokine that participates in the development of many inflammatory disorders, including those that contribute to cardiovascular disease.<sup>10–14</sup> MIF amplifies the proinflammatory cascade and it controls the “set point” and the magnitude of inflammatory responses (eg, JNK1 response).<sup>10,15</sup> In a recent study, we showed that MIF can exert chemokine-like functions, thereby enhancing the tissue infiltration of macrophages during atherogenesis.<sup>16</sup>

Here, we have investigated whether genetic deletion of *mif* would result in a lower systemic and/or lower WAT-specific inflammation and whether reducing MIF-dependent inflammation would prevent the development of IR, glucose intolerance, and associated cardiovascular disease. The LDL receptor-deficient mouse (Ldlr<sup>-/-</sup>) was chosen as a model because IR and atherosclerosis develop sequentially<sup>17</sup> and under the mild conditions of a chow diet thereby mimicking the slow progression of disease in humans. Glucose tolerance testing and hyperinsulinemic-euglycemic clamp analysis in combination with functional, genome-wide pathway analysis, and immunohistochemistry enabled us to explore for the first time the role of MIF in a chronic setting of acquired IR and atherosclerosis.

## Materials and Methods

An expanded Materials and Methods section is available in the Online Data Supplement at <http://circres.ahajournals.org>.

All mouse lines used had a C57BL/6 background. Atherosclerosis-prone Ldlr<sup>-/-</sup> mice were crossbred with MIF-deficient mice (Mif<sup>-/-</sup>) mice<sup>18</sup> to generate Ldlr<sup>-/-</sup>Mif<sup>-/-</sup> mice. Male littermates derived from crossbreeding of Ldlr<sup>-/-</sup>Mif<sup>+/-</sup> mice were used for the metabolic cage experiments, glucose tolerance tests, insulin tolerance tests, the hyperinsulinemic euglycemic clamp analysis, and the atherosclerosis experiments. Mice of both gender were used for the cytokine stimulation experiments.

Human (hu)CRP transgenic mice were challenged with IL-1β as described.<sup>19</sup> Animal experiments were ethically approved by an independent Animal Care and Use Committee and were in compliance with European Community specifications regarding the use of laboratory animals.

## Results

### Effect of MIF Deficiency on Lipids and Metabolic Markers

Ldlr<sup>-/-</sup> mice and Mif<sup>-/-</sup>Ldlr<sup>-/-</sup> littermates were fed a chow diet for 35 weeks and risk factors of the metabolic syndrome were monitored over time. The plasma levels of cholesterol, triglycerides and free fatty acids were comparable in both groups of mice (the Table shows values at t=12 and t=35 weeks). Ldlr<sup>-/-</sup> and Mif<sup>-/-</sup>Ldlr<sup>-/-</sup> mice also had similar lipoprotein profiles, indicating that the presence or absence of MIF does not affect the level of very-low-density lipoprotein (VLDL), LDL, and HDL (Figure 1A).

Fasting plasma insulin concentrations at 12 weeks of age tended to be lower in Mif<sup>-/-</sup>Ldlr<sup>-/-</sup> (0.77±0.09 versus 1.27±0.38 mmol/L), and this difference became significant at week 35 because insulin levels increased strongly in Ldlr<sup>-/-</sup> (4.0±0.7 mmol/L) but only moderately in Mif<sup>-/-</sup>Ldlr<sup>-/-</sup> mice (1.9±0.2 mmol/L; Figure 1B). A similar picture was also obtained for glucose: whereas fasting blood glucose levels were comparable at 12 weeks of age (8.0±1.6 mmol/L in Ldlr<sup>-/-</sup> and 7.6±1.4 mmol/L in Mif<sup>-/-</sup>Ldlr<sup>-/-</sup> mice), with increasing age, a significant difference emerged at week 35 because glucose levels increased in Ldlr<sup>-/-</sup> mice (10.2±2.0 mmol/L) while remaining low in Mif<sup>-/-</sup>Ldlr<sup>-/-</sup> mice (7.3±1.0 mmol/L) (Figure 1C).

Calculation of the HOMA index as a measure of IR in week 12 and 35 revealed a strong increase in Ldlr<sup>-/-</sup> mice (from 0.3±0.1 to 1.9±0.4). In contrast, HOMA hardly increased in Mif<sup>-/-</sup>Ldlr<sup>-/-</sup> (from 0.2±0.05 to 0.6±0.02) (Figure 1D). These data show that Mif<sup>-/-</sup>Ldlr<sup>-/-</sup> mice are protected from developing hyperinsulinemia and hyperglycemia, which suggests that MIF has a role in the development of IR.

There was no difference in food intake between the groups during the treatment, and Mif<sup>-/-</sup>Ldlr<sup>-/-</sup> mice had a slightly lower body weight (not significant) (Table). Also, when the treatment was prolonged (up to 52 weeks), there was no significant effect on body weight: both groups became obese and the average body weight was 46.9±5.6 g in Ldlr<sup>-/-</sup> and 44.1±7.2 g in Mif<sup>-/-</sup>Ldlr<sup>-/-</sup>. The mass of subcutaneous, visceral, and epididymal fat was also comparable in Ldlr<sup>-/-</sup> and Mif<sup>-/-</sup>Ldlr<sup>-/-</sup> mice (subcutaneous: 1.45±0.37 versus

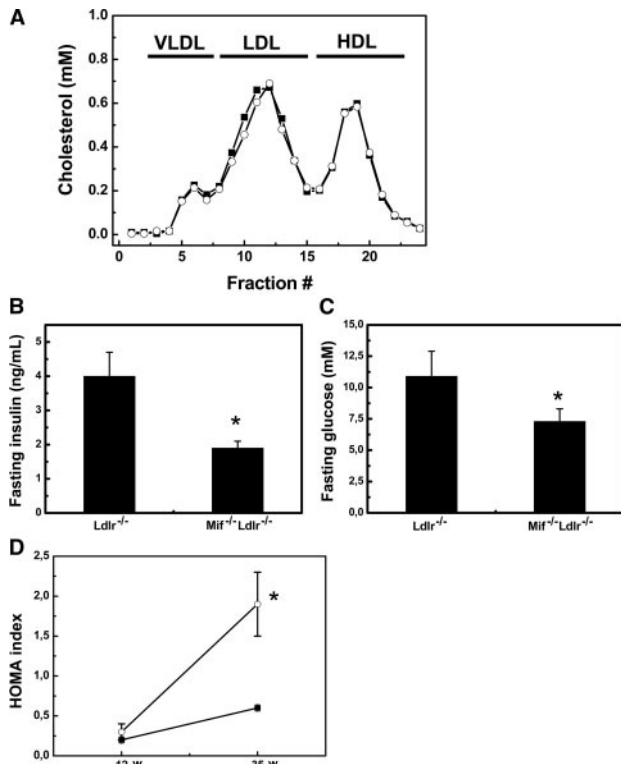


**Figure 1.** A, Lipoprotein profiles of Ldlr<sup>-/-</sup> (open circles) and Mif<sup>-/-</sup>Ldlr<sup>-/-</sup> (solid squares) mice fed a chow diet at 35 weeks. B through D, Average fasting plasma insulin levels (B), average fasting whole blood glucose levels (C), and HOMA values (D) of Ldlr<sup>-/-</sup> (open) and Mif<sup>-/-</sup>Ldlr<sup>-/-</sup> (solid) mice at the ages of 12 and 35 weeks. Data are expressed as means±SD (n≥8 per genotype). \*P<0.05.

1.79±0.61 g; visceral: 0.71±0.12 versus 0.66±0.30 g; epididymal: 1.38±0.47 versus 1.26±0.43 g in week 52), and plasma leptin levels were similar in the two strains (Table).

In an independent experiment, the metabolic performance of Ldlr<sup>-/-</sup> and Mif<sup>-/-</sup>Ldlr<sup>-/-</sup> mice was analyzed in more detail. Mice were housed individually in computerized metabolic cages with free access to water and chow. There was no significant difference in voluntary activity, food intake, water consumption, O<sub>2</sub> consumption, and CO<sub>2</sub> production (Online Figure I). In both groups, the respiratory exchange rate (RER) varied between 0.9 (night) and 1 (day), indicating that mice predominantly used glucose in chow as an energy substrate.

### MIF Deficiency Lowers Chronic Inflammation and Reduces the Magnitude of the Inflammatory Response

SAA is a circulating inflammation marker produced by liver and adipose tissue. SAA levels were significantly lower in Mif<sup>-/-</sup>Ldlr<sup>-/-</sup> mice already at week 12 (Table), ie, at a time point at which Ldlr<sup>-/-</sup> and Mif<sup>-/-</sup>Ldlr<sup>-/-</sup> still had comparable levels of insulin and glucose. Whereas SAA levels strongly increased in Ldlr<sup>-/-</sup> (up to 109±14 μg/mL at 35 weeks), they remained low in Mif<sup>-/-</sup>Ldlr<sup>-/-</sup> (10±7 μg/mL). Mif<sup>-/-</sup>Ldlr<sup>-/-</sup> also displayed significantly lower levels of fibrinogen, a liver-specific marker of inflammation (Table). Our finding that MIF influences the inflammatory status was

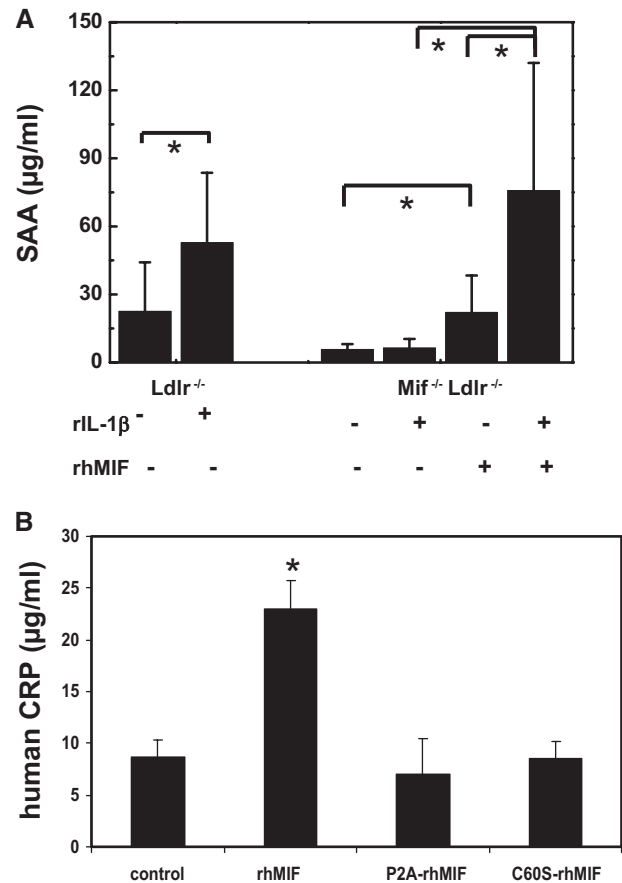


**Figure 2.** A, Plasma SAA levels 18 hours after stimulation with recombinant IL-1β (100 000 U/mouse). Plasma SAA levels started to increase 8 hours after stimulation and returned to baseline after 30 hours (data not shown). In Mif<sup>-/-</sup>Ldlr<sup>-/-</sup> mice, MIF was reconstituted by IP administration of recombinant human MIF protein (rhMIF) (10 μg of LPS-free rhMIF [ $<1$  pg of endotoxin per microgram of rhMIF protein, as assessed by Limulus Amoebocyte Lysate assay]). B, Human CRP levels in human CRP transgenic mice 18 hours after stimulation with either rhMIF or P2A-rhMIF lacking tautomerase activity or C60S-rhMIF lacking oxidoreductase activity (all 10 μg; IP). Data are means±SD (n≥9 per treatment group). \*P<0.05.

also confirmed in normolipidemic C57BL/6 mice. Plasma SAA and fibrinogen concentrations were 70±11 μg/mL and 3.3±1.1 mg/mL in MIF-expressing C57BL/6 whereas MIF-deficient littermates displayed significantly lower levels (7±1 μg/mL and 2.7±0.8 mg/mL, P<0.05; not shown).

Stimulation experiments with a prototypic trigger of inflammation, IL-1β, revealed that MIF also determined the magnitude of an inflammatory response. Ldlr<sup>-/-</sup> and Mif<sup>-/-</sup>Ldlr<sup>-/-</sup> were intraperitoneally challenged with IL-1β (125.000 U/25 g body weight). Plasma SAA was quantified 18 hours after IL-1β injection, which is a time point for which stimulation previously had been determined to be maximal (not shown). IL-1β stimulation resulted in an inflammatory response and significantly increased plasma SAA levels in Ldlr<sup>-/-</sup> mice (Figure 2A). In Mif<sup>-/-</sup>Ldlr<sup>-/-</sup> mice, however, plasma SAA remained low, even at a later time point (not shown). Reconstitution of Mif<sup>-/-</sup>Ldlr<sup>-/-</sup> mice with recombinant (r)MIF (single IP injection of 10 μg of lipopolysaccharide [LPS]-free rMIF 15 hours before IL-1β induction) resulted in

baseline and IL-1-stimulated SAA levels that were comparable to those observed in *Ldlr*<sup>-/-</sup> mice (Figure 2A).

The expression of human CRP, which is a sensitive marker of chronic inflammation and a predictor of metabolic and cardiovascular disease, was induced by rMIF as shown in Figure 2B: mice transgenic for human CRP (CRPtg) responded to rMIF (10 μg IP) with a significant increase (2.6-fold) in plasma CRP concentrations. The effect of MIF on CRP was time- and dose-dependent and maximal 18 hours after stimulation (not shown). MIF was less potent than IL-1β (9-fold increase of CRP; not shown), which is a well-established stimulator of CRP in this model.<sup>19a</sup> Protein mutants of MIF, ie, C60S-MIF or P2A-MIF, that lack the intrinsic catalytic activity of MIF and have been found to also lack inflammatory activities<sup>20,21</sup> did not stimulate CRP expression in CRPtg mice, thereby confirming that the effect of MIF on CRP was specific (Figure 2B). Consistent with this notion, rMIF but not the mutant proteins stimulated human CRP promoter activity in human HuH7 hepatoma cells transiently transfected with a plasmid containing a 300-bp fragment of the human CRP promoter cloned in front of a luciferase reporter gene. The CRP promoter-activating effect of MIF alone was ≈2-fold (not shown) and additive to the stimulating effect of IL-1 (Online Figure II). Also, MIF stimulated the basal and IL-1-induced activity of the promoter of IL-6, the principle cytokine inducer of CRP (Online Figure II).

### MIF Deficiency Protects Against the Development of Glucose Intolerance and IR

To examine whether a reduction in chronic, low-grade inflammation by deleting *mif* would affect the development of IR, we subjected *Ldlr*<sup>-/-</sup> and *Mif*<sup>-/-</sup>*Ldlr*<sup>-/-</sup> mice (12 weeks of age) to glucose tolerance and insulin tolerance tests. In the presence of MIF, peak glucose levels normalized later and *Ldlr*<sup>-/-</sup> mice had a significantly higher area under the curve (AUC) than *Ldlr*<sup>-/-</sup>*Mif*<sup>-/-</sup> (AUC: 817±353 versus 507±174; *P*<0.05; Figure 3A). The difference in glucose tolerance became even more pronounced at later time points. At 35 weeks, the AUC was 1225±397 in *Ldlr*<sup>-/-</sup> but stayed at 519±194 in *Ldlr*<sup>-/-</sup>*Mif*<sup>-/-</sup> (*P*<0.001; Figure 3B). Insulin levels did not differ significantly during glucose tolerance testing (not shown).

Subsequent insulin tolerance tests revealed that the clearance of plasma glucose occurred more efficiently (ie, more rapidly within the first 15 minutes; *P*<0.05) in *Ldlr*<sup>-/-</sup>*Mif*<sup>-/-</sup> mice (Figure 3C), which suggests that a difference in insulin sensitivity may exist. In line with this notion, hyperinsulinemic-euglycemic clamp analysis showed that the glucose infusion rate in *Ldlr*<sup>-/-</sup>*Mif*<sup>-/-</sup> mice was greater than in *Ldlr*<sup>-/-</sup> (14.0±3.4 versus 8.6±3.7 mg/kg per minute; *P*<0.05), indicating that the presence of MIF may promote the development of IR (Figure 3D).

### MIF Deficiency Reduces the Inflammatory State of WAT

Because the circulating levels of inflammatory markers were lower in *Mif*<sup>-/-</sup>*Ldlr*<sup>-/-</sup> mice, we analyzed the inflammatory status of liver and WAT. Western blot analysis of tissue homogenates showed that MIF is expressed in liver and WAT

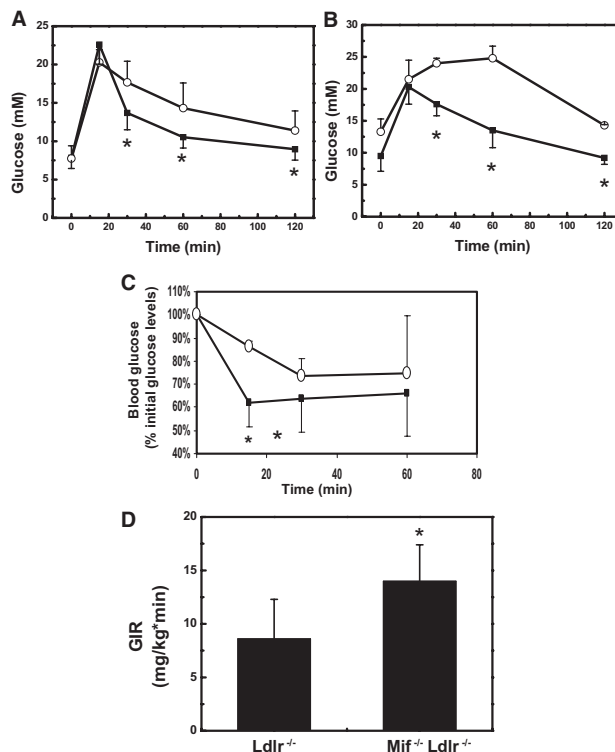


**Figure 3.** A, Glucose tolerance test in 12-week-old *Ldlr*<sup>-/-</sup> (open) and *Mif*<sup>-/-</sup>*Ldlr*<sup>-/-</sup> (solid) mice (2 g of glucose per kg body weight; IP). Blood glucose levels were monitored at time points indicated. B, as in A but 35-week-old mice. C, Insulin tolerance test in 12-week-old *Ldlr*<sup>-/-</sup> (open circles) and *Mif*<sup>-/-</sup>*Ldlr*<sup>-/-</sup> (solid squares) mice. Animals were treated with insulin (0.5 U per 25 g body weight; IP). D, Assessment of whole body insulin resistance by euglycemic hyperinsulinemic clamp analysis at 12 weeks of age. Glucose infusion rate (GIR) is shown. Data are means±SD (n≥10 per genotype); \**P*<0.05.

of *Ldlr*<sup>-/-</sup> mice (Figure 4A). A parallel immunohistochemical (IHC) analysis demonstrated MIF immunoreactivity in all cell types present in these tissues (not shown).

The liver tissue of *Ldlr*<sup>-/-</sup> mice showed slight c-Jun immunoreactivity, but there was no significant difference in either c-Jun or p-c-Jun immunoreactivity when these mice were compared to *Mif*<sup>-/-</sup>*Ldlr*<sup>-/-</sup> littermates (not shown). The expression of hepatic genes encoding enzymes that control glucose homeostasis/de novo synthesis (phosphoenolpyruvate carboxykinase, glucose-6-phosphatase) also was comparable in both groups (not shown).

Histological analysis of WAT revealed smaller adipocytes in *Mif*<sup>-/-</sup>*Ldlr*<sup>-/-</sup> mice when compared to *Ldlr*<sup>-/-</sup>. This difference was observed already at a young age (12 to 18 weeks), ie, before the infiltration of macrophages into WAT. Computerized quantification of adipocyte size demonstrated a significant difference in young (Online Figure III) and old (25 to 35 weeks) animals (Figure 4B).

Specific immunostaining of macrophages (anti-MAC3) showed that the WAT of 25- to 35-week-old *Mif*<sup>-/-</sup>*Ldlr*<sup>-/-</sup> contained significantly fewer macrophages and fewer crown-like structures than the WAT of *Ldlr*<sup>-/-</sup> (Figure 4C and Online Figure IV). Analysis of the expression of genes that are characteristic for M1-type (CXCR4; CCR2) and M2-type (Ly-6C; Mrc1) macrophage responses in WAT by Affymetrix

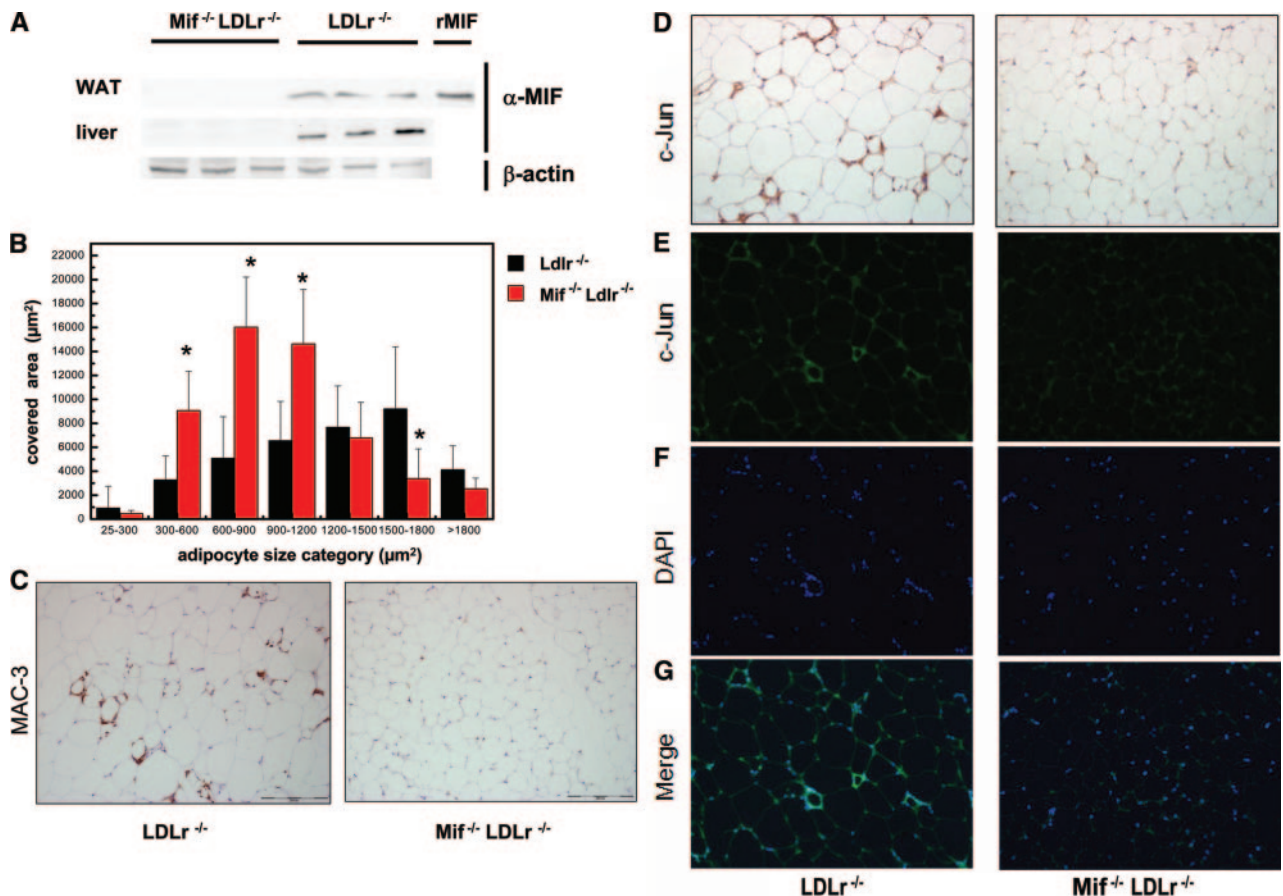


**Figure 4.** A, Western blot analysis of Mif in tissue homogenates of *Ldlr*<sup>-/-</sup> and *Mif*<sup>-/-</sup>*Ldlr*<sup>-/-</sup> mice (25 to 35 w). B, Computerized quantification of adipocyte size in *Ldlr*<sup>-/-</sup> (black bars) and *Mif*<sup>-/-</sup>*Ldlr*<sup>-/-</sup> (red bars) mice. Adipocytes were classified into groups on basis of their size (x axis). An identical total area was analyzed by the software. The peak size of adipocytes in *Ldlr*<sup>-/-</sup> was 1500 to 1800 μm<sup>2</sup>, whereas in *Mif*<sup>-/-</sup>*Ldlr*<sup>-/-</sup> mice, it was only 600 to 900 μm<sup>2</sup>. Data shown are means ± SD (n ≥ 8). \*P < 0.05. C through F, Representative photomicrographs of epididymal adipose tissue from *Ldlr*<sup>-/-</sup> and *Mif*<sup>-/-</sup>*Ldlr*<sup>-/-</sup> mice (n ≥ 7 per genotype; 4 cross-sections per mouse) stained with a macrophage-specific antibody (MAC-3) (C), a c-Jun-specific antibody detected with Nova Red (D), a c-Jun-specific antibody detected with fluorescent-labeled secondary antibody (E), or with DAPI (for nuclei) (F). G, Merged photomicrographs showing that c-Jun-immunoreactivity (IR) is nuclear.

microarray (Online Table I) revealed that the M1/M2 ratio tended to be lower in *Mif*<sup>-/-</sup>*Ldlr*<sup>-/-</sup> mice (not shown). In an independent RT-PCR analysis (n = 6), we found that the CCR2/Ly-6C mRNA expression ratio is 54% (P < 0.05) lower in *Mif*<sup>-/-</sup>*Ldlr*<sup>-/-</sup>. Plasma adiponectin levels were comparable in *Mif*<sup>-/-</sup>*Ldlr*<sup>-/-</sup> (10.4 ± 1.8 μg/mL) and *Ldlr*<sup>-/-</sup> mice (11.2 ± 2.6 μg/mL).

In *Ldlr*<sup>-/-</sup> mice, pronounced c-Jun immunoreactivity (Figure 4D) was observed in MAC3-positive areas as well as in adipocytes. Merging the immunofluorescent signals of c-Jun and nuclear DAPI revealed that a substantial amount of c-Jun was associated to the nucleus (Figure 4E through 4G). Nuclear c-Jun immunoreactivity was predominantly found in adipocytes that were in close proximity to macrophages/crown-like structures but such staining was less evident in more distant adipocytes. In WAT from *Ldlr*<sup>-/-</sup>*Mif*<sup>-/-</sup> mice, c-Jun immunoreactivity was less intense and mainly cytosolic.

To study a role of MIF in the inflammatory responsiveness of macrophages, thioglycollate-elicited macrophages were isolated from wild-type and MIF<sup>-/-</sup> mice and cells were stimulated with LPS. Supernatants were harvested after 6 and 12 hours and assayed for IL-6 by ELISA. MIF-deficient

macrophages showed a significantly impaired responsiveness as demonstrated by significantly less IL-6 production compared to wild-type macrophages (Online Figure V).

A comparison of WAT from *Mif*<sup>-/-</sup>*Ldlr*<sup>-/-</sup> and *Ldlr*<sup>-/-</sup> by functional microarray analysis across pathways showed that the major changes in gene expression occur in the functional categories “cell signaling,” “cell cycle control,” “immune response,” and “lipid metabolism.” Within the category “cell signaling,” the insulin-sensitive processes “leptin signaling via JAK/STAT and MAPK cascades” and “IGF-R1 signaling” were differentially affected (Online Table I). These data, considered together with the IHC analysis of c-Jun, suggest an effect of MIF on insulin sensitivity.

As a direct test of the influence of MIF on the insulin signaling cascade, we injected insulin (IP; 0.5 U insulin/25 g body weight) into *Ldlr*<sup>-/-</sup> and *Mif*<sup>-/-</sup>*Ldlr*<sup>-/-</sup> littermates. Mice were euthanized 10 minutes after injection (insulin dose and time point of euthanasia had been optimized in previous scouting experiments) and the IRS1-associated phosphatidylinositol (PI)3-kinase activity was determined as a functional measure of the insulin signaling route. PI3-kinase activity was significantly higher in WAT of *Mif*<sup>-/-</sup>*Ldlr*<sup>-/-</sup> mice

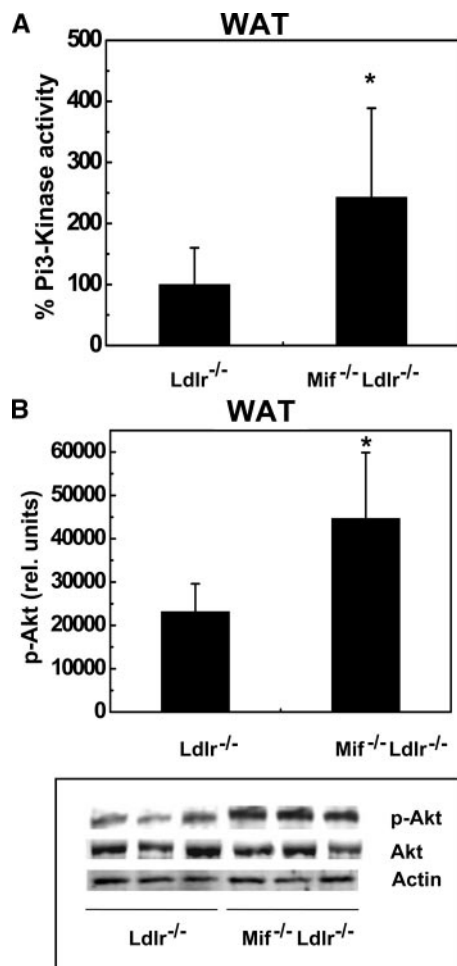


**Figure 5.** A, PI3-kinase activity in WAT from 25- to 35-week-old Ldlr<sup>-/-</sup> and Ldlr<sup>-/-</sup> Mif<sup>-/-</sup> mice euthanized precisely 10 minutes after treatment with 0.5 U of insulin per 25 g body weight. B, p-AKT levels in WAT of Ldlr<sup>-/-</sup> and Ldlr<sup>-/-</sup> Mif<sup>-/-</sup> mice assessed by Western blotting (a representative blot is shown). Data are means $\pm$ SD (n $\geq$ 7 per genotype). \* $P$ <0.05.

when compared to Ldlr<sup>-/-</sup> mice (Figure 5A). The biological relevance of this effect was supported further by the higher levels of phospho-AKT, a downstream effector of PI3-kinase, in WAT of Mif<sup>-/-</sup>Ldlr<sup>-/-</sup> mice (Figure 5B). No difference in PI3-kinase activity and phospho-AKT levels in liver and muscle were observed (Online Figure VI).

### MIF Deficiency Blocks Macrophage Infiltration into WAT

Pathway analysis of the WAT transcriptome dataset showed that the presence of MIF was significantly associated with the inflammatory processes “IL-1 and IL-6 signaling,” “ERK activation,” “IL-3 activation and signaling,” and “cell adhesion” (all  $P$ <0.05; Online Table D). Consistent with the enhanced inflammatory status of MIF-expressing Ldlr<sup>-/-</sup> mice, the genes encoding for chemokines (Ccl2, Ccl9, Ccr5, Ccl6), proteases (Mmp12), complement components (C1qb, C1qa, C3ar3, C3ar1), acute phase proteins (Mup-1, Orm2, SAA3), and cell adhesion/immune cell recruitment factors (Cd9, Cd44, Cd84, Cd72) also were significantly ( $P$ <0.01) upregulated, suggesting that MIF promotes the recruitment of

immune cells into adipose tissue. To substantiate this observation, we measured the expression level of proteins that mediate monocyte/macrophage recruitment into WAT. Circulating levels of vascular cell adhesion molecule (VCAM)-1 and intercellular adhesion molecule (ICAM)-1 were significantly lower in Mif<sup>-/-</sup>Ldlr<sup>-/-</sup> mice compared to Ldlr<sup>-/-</sup> (Figure 6A and 6B). IHC staining of the cell adhesion molecules ICAM and CD44 in cross-sections of WAT showed pronounced ICAM and CD44 levels in Ldlr<sup>-/-</sup> mice. CD44 was predominantly detected in MAC3-positive cells of crown-like structures. ICAM-1 and CD44 staining was markedly and significantly reduced in Mif<sup>-/-</sup>Ldlr<sup>-/-</sup> mice (Figure 6C and 6D and Online Figure IV), providing a molecular rationale for the lower macrophage content in WAT.

### MIF Deficiency Reduces Atherosclerosis Associated With IR

Atherosclerosis developed after glucose intolerance/IR and was analyzed in mice maintained on a chow diet for 52 weeks. The aortic plaque load (determined by en face oil red O staining) of Mif<sup>-/-</sup>Ldlr<sup>-/-</sup> mice was lower than in Ldlr<sup>-/-</sup> (Figure 7A). Mif<sup>-/-</sup>Ldlr<sup>-/-</sup> also displayed significantly less atherosclerosis in the aortic valve area of the aortic root (Figure 7B). Analysis of the lesional content of monocytes/macrophages in cross-sections of the aortic root demonstrated a significant reduction in the numbers of these cells in Ldlr<sup>-/-</sup>Mif<sup>-/-</sup> mice (reduced by 5.1-fold  $P$ <0.05; Figure 7C and data not shown).

These data are consistent with the observed effects of MIF in WAT, and they support the conclusion that MIF deficiency impairs the accumulation of monocytes/macrophages in the vascular wall, which is a fundamental, pathological feature necessary for the development of atherosclerosis.

### Discussion

MIF plays pivotal roles in inflammatory diseases and atherogenesis,<sup>13,14</sup> but it has remained unclear whether MIF is causally involved in the development of metabolic disorders associated with obesity and the metabolic syndrome. We show herein that genetic deletion of MIF blocks the development of glucose intolerance, IR, and associated atherosclerotic disease. Importantly, MIF deficiency reduces macrophage infiltration into WAT and lowers both tissue-specific and systemic chronic inflammation without affecting obesity (adiposity) and lipid risk factors. The data indicate that the adipocyte and the macrophage are of importance to the effects observed by MIF deficiency. To our knowledge, the present study provides the first experimental evidence for the direct involvement of MIF in the evolution of IR/glucose intolerance, and it is consistent with previous reports showing that MIF is a key element in atherogenesis.<sup>13,14</sup> Our observation that MIF deficiency reduces WAT inflammation and selectively improves the insulin sensitivity of this tissue is consistent with the finding that glucose uptake into WAT is increased in Mif<sup>-/-</sup> mice under conditions of severe inflammation (LPS-induced endotoxemia) with glucose uptake of skeletal muscle and hepatic glucose production being unaffected.<sup>22</sup>

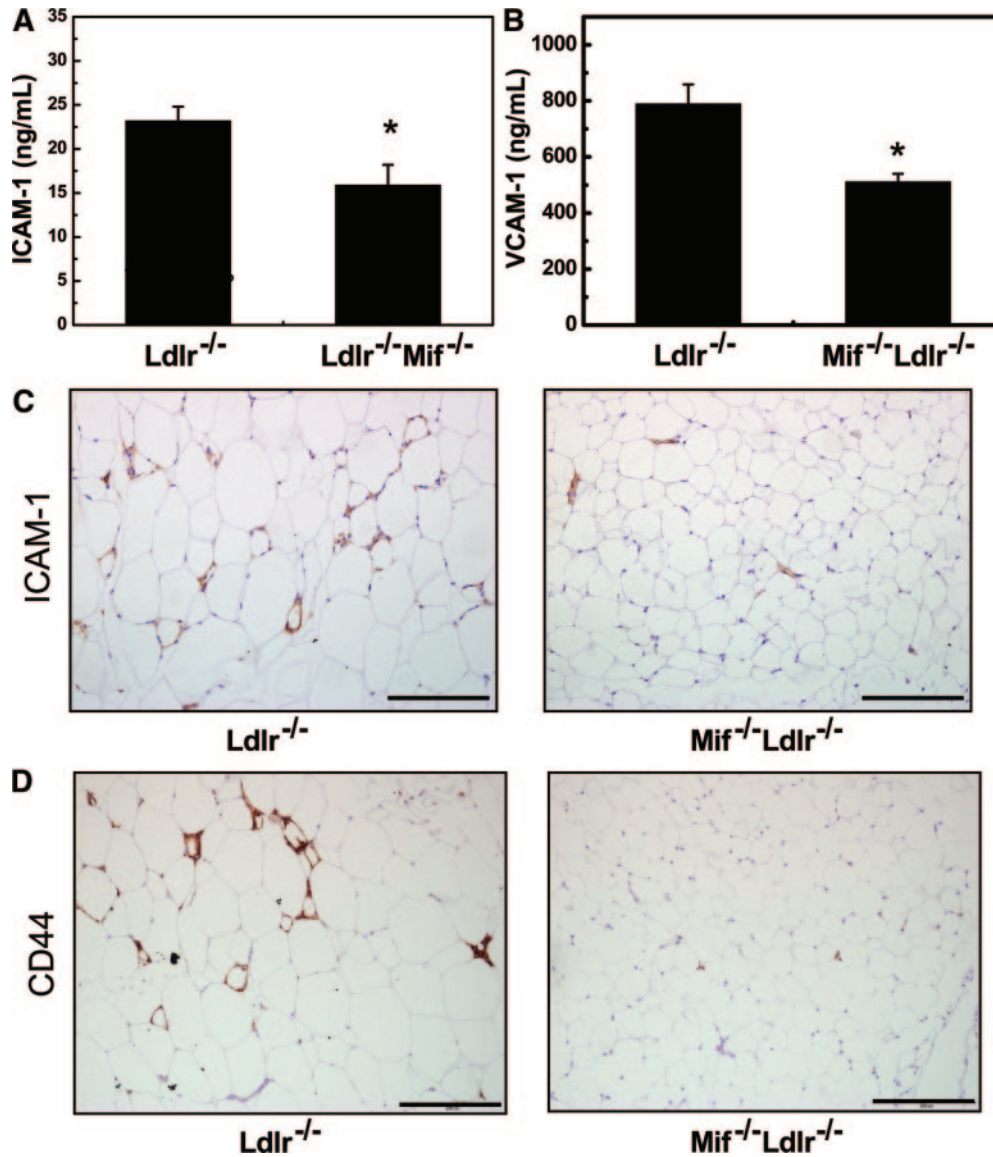


**Figure 6.** A and B, Plasma levels of ICAM-1 (A) and VCAM-1 (B) in 25 to 35-week-old Ldlr<sup>-/-</sup> and Mif<sup>-/-</sup>Ldlr<sup>-/-</sup> mice. Data are means ± SD (n ≥ 8 per genotype). \*P < 0.05. C and D, Representative photomicrographs of epididymal adipose tissue from Ldlr<sup>-/-</sup> and Mif<sup>-/-</sup>Ldlr<sup>-/-</sup> mice (n ≥ 7 each) stained with an antibody specific for ICAM-1 (C) or an antibody specific for CD44 (D).

Chronic low-grade inflammation is considered to be an important risk factor of metabolic and cardiovascular diseases, but it is unclear how it can be manipulated without severe consequences to the organism.<sup>23</sup> Metabolic and immune response pathways are evolutionarily linked, and, therefore, modulation of inflammatory risk factors often affects metabolic risk factors and vice versa.<sup>7,24</sup> For example, deletion of inflammatory cytokines such as IL-1 $\alpha$ , IL-6, IL-18, and tumor necrosis factor- $\alpha$  can result in a significant increase in plasma cholesterol.<sup>24</sup> Here, we show that MIF deficiency lowers the inflammatory reactivity without affecting typical metabolic risk factors including plasma triglycerides, free fatty acids, VLDL, LDL, HDL, body weight, adipose mass, voluntary activity, and metabolic performance. Compared to Ldlr<sup>-/-</sup> mice, Mif<sup>-/-</sup>Ldlr<sup>-/-</sup> mice display lower levels of systemic (SAA, fibrinogen) and vascular (ICAM-1, VCAM-1) inflammation markers, and their WAT

contains less macrophages, nucleus-associated c-Jun, ICAM-1, and CD44. One reason for the observed selective reduction in inflammation may be that MIF does not participate in the interface that links metabolic to inflammatory pathways (“metaflammation” pathways<sup>23</sup>) and that the role of MIF within the inflammatory cascade is mainly to amplify and enhance existing inflammatory signals. This amplifier function may explain the large differences in local WAT-specific inflammation observed in this study. Adipose tissue is considered to be an important site for the production of inflammatory mediators,<sup>1,23</sup> and it is possible that the lower WAT inflammation observed in the setting of MIF deficiency is attributable to both a lower systemic inflammatory response and to a loss of amplifying signals for cytokine (IL-6) and acute phase (CRP, SAA, fibrinogen) responses in the liver. This also illustrates that difference in inflammatory status in Mif<sup>-/-</sup>Ldlr<sup>-/-</sup> and Ldlr<sup>-/-</sup> can be either primary

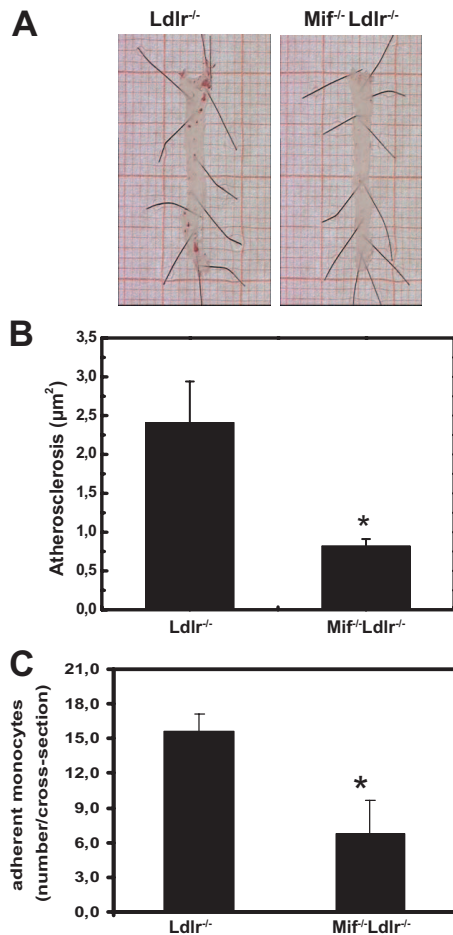


**Figure 7.** A, Representative photomicrographs of longitudinally opened en face oil red O-stained aortas from Ldlr<sup>-/-</sup> and Mif<sup>-/-</sup>Ldlr<sup>-/-</sup> mice (52 weeks of age). B and C, Analysis of atherosclerosis (B) and monocyte adhesion (C) in the aortic valve area of the aortic root. Data are means±SD (n=7 per genotype). \*P<0.05.

(ie, a direct effect of MIF) or secondary (ie, a consequence of a MIF effect on another factor).

The specific effect of MIF deficiency on the inflammatory state (but not on lipid/metabolic risk factors) enabled us to study the consequences of a prolonged, selective reduction of inflammation. Our results clearly demonstrate that lowering chronic inflammation per se is an effective strategy to block the development of metabolic as well as cardiovascular disease. Genetic deletion of MIF thus produces a different phenotype than that resulting from genetic deficiency of CCR2, which encodes a high-affinity ligand of CCL2/MCP-1 that also regulates macrophage infiltration into WAT in the context of IR.<sup>25</sup> Genetic deficiency in CCR2 reduces food intake and adiposity, thereby attenuating the development of obesity. Our data show that WAT inflammation and the development of IR can be reduced significantly without affecting the development of obesity.

Recent epidemiological data provide support for a role for MIF in the development of IR in humans. Herder et al reported a strong positive association between systemic concentrations of MIF and impaired glucose tolerance and T2D.<sup>26</sup> They also showed that the MIF genotype

rs1007888CC is associated with increased circulating MIF levels and an increased T2D risk.<sup>27</sup> Interestingly, in male participants, MIF levels were significantly associated with high CRP and IL-6 levels. We found that MIF-expressing mice (independent of the Ldlr<sup>-/-</sup> background) display higher levels of fibrinogen, an IL-6-inducible liver-derived acute phase protein (APP), and SAA, which can be viewed as the murine counterpart of CRP. We also demonstrate that MIF is involved in the constitutive and IL-1-induced expression of SAA. This effect and the finding that MIF stimulates the expression of human CRP in vivo as shown in human CRP transgenic mice have not been reported so far.

The role of MIF in the regulation of acute phase genes (eg, CRP, SAA, fibrinogen) has not been analyzed systematically. A positive effect of MIF on APP is of great importance because these proteins are not only powerful predictors of disease but also participate in pathophysiological processes leading to the formation of atherosclerotic lesions.<sup>8</sup> Possible sources of proatherogenic APP production are WAT and liver. It is well established that very powerful cytokine inducers of hepatic APP expression are IL-1β and IL-6,<sup>9,28</sup> both of which are increasingly expressed during ageing in mouse WAT.<sup>9</sup> It is thus possible that the observed differences in APP levels are a consequence of a local effect of MIF in WAT (eg, on IL-6 release by this tissue). However, from a mechanistic point of view, the positive association between MIF and APP plasma levels remain unclear because studies that could provide a molecular rationale are lacking. A possible explanation may be that MIF controls a transcription factor shared by the various APP. We have shown that immunoneutralization of MIF lowers plasma fibrinogen and IL-6 levels and reduces the expression level of C/EBPβ, a common transcription factor.<sup>29</sup> C/EBPβ is not only a positive regulator of IL-6, fibrinogen, SAA, and CRP but also a transcription factor for the adhesion molecules VCAM-1 and ICAM-1,<sup>30</sup> each of which was affected in this study in a MIF-dependent way.

Taken together, our observations support the overall physiological importance of chronic inflammation in the pathogenesis of IR and associated atherosclerosis. Given that the metabolic parameters studied (eg, triglycerides, free fatty acids, VLDL, LDL, HDL, body weight, and adiposity) were unchanged in Ldlr<sup>-/-</sup> and Mif<sup>-/-</sup>Ldlr<sup>-/-</sup> mice, MIF may represent a unique therapeutic target for the specific reduction of WAT inflammation and the ensuing development of cardiovascular and metabolic diseases.

### Acknowledgments

We thank Annie Jie and Karin Toet for excellent bioinformatical and analytic help.

### Sources of Funding

This study was supported by the Dutch Organization for Scientific Research (NWO-Zon-MW; VENI-016.036.061 to R.K.; VENI-916-36-071 and VIDI-917.76.301 to P.J.V.), the Dutch Heart Foundation (grant 2002B102 to L.V.), the TNO Personalized Health research program (to R.K., M.v.E., T.K.), the Nutrigenomics Consortium, the Centre for Medical Systems Biology (grant 115) in the framework of the Netherlands Genomics Initiative (to J.d.V.-v.d.W. and K.W.v.D.), the NIH (to R.B.), the German Research Council (SFB 542/TP-A7 and DFG-FOR809/P1 to J.B.; Fi712/2-1 to G.F.-R.), the

Cologne Fortune Program of the Medical Faculty of Cologne University (to G.F.-R.), and the European Commission (grant COST-BM0602 to D.M.O.).

## Disclosures

None.

## References

- Neels JG, Olefsky JM. Inflamed fat: what starts the fire? *J Clin Invest.* 2006;116:33–35.
- Bansilal S, Farkouh ME, Fuster V. Role of insulin resistance and hyperglycemia in the development of atherosclerosis. *Am J Cardiol.* 2007;19:99:6B–14B.
- Xu H, Barnes GT, Yang Q, Tan G, Yang D, Chou CJ, Sole J, Nichols A, Ross JS, Tartaglia LA, Chen H. Chronic inflammation in fat plays a crucial role in the development of obesity-related insulin resistance. *J Clin Invest.* 2003;112:1821–1830.
- Festa A, D'Agostino R Jr, Tracy RP, Haffner SM. Elevated levels of acute-phase proteins and plasminogen activator inhibitor-1 predict the development of type 2 diabetes: the insulin resistance atherosclerosis study. *Diabetes.* 2002;51:1131–1137.
- Festa A, D'Agostino R Jr, Howard G, Mykkanen L, Tracy RP, Haffner SM. Chronic subclinical inflammation as part of the insulin resistance syndrome: the Insulin Resistance Atherosclerosis Study (IRAS). *Circulation.* 2000;102:42–47.
- Kaneto H, Nakatani Y, Miyatsuka T, Kawamori D, Matsuoka TA, Matsuhisa M, Kajimoto Y, Ichijo H, Yamasaki Y, Hori M. Possible novel therapy for diabetes with cell-permeable JNK-inhibitory peptide. *Nat Med.* 2004;10:1128–1132.
- Kleemann R, Verschuren L, van Erk MJ, Nikolsky Y, Cnubben NH, Verheij ER, Smilde AK, Hendriks HF, Zadelaar S, Smith GJ, Kaznacheev V, Nikolskaya T, Melnikov A, Hurt-Camejo E, van der GJ, van OB, Kooistra T. Atherosclerosis and liver inflammation induced by increased dietary cholesterol intake: a combined transcriptomics and metabolomics analysis. *Genome Biol.* 2007;8:R200.
- O'Brien KD, McDonald TO, Kunjathoor V, Eng K, Knopp EA, Lewis K, Lopez R, Kirk EA, Chait A, Wight TN, Debeer FC, Leboeuf RC. Serum amyloid A and lipoprotein retention in murine models of atherosclerosis. *Arterioscler Thromb Vasc Biol.* 2005;25:785–790.
- Wu D, Ren Z, Pae M, Guo W, Cui X, Merrill AH, Meydani SN. Aging up-regulates expression of inflammatory mediators in mouse adipose tissue. *J Immunol.* 2007;179:4829–4839.
- Lue H, Kleemann R, Calandra T, Roger T, Bernhagen J. Macrophage migration inhibitory factor (MIF): mechanisms of action and role in disease. *Microbes Infect.* 2002;4:449–460.
- Zernecke A, Bernhagen J, Weber C. Macrophage migration inhibitory factor in cardiovascular disease. *Circulation.* 2008;117:1594–1602.
- Miller EJ, Li J, Leng L, McDonald C, Atsumi T, Bucala R, Young LH. Macrophage migration inhibitory factor stimulates AMP-activated protein kinase in the ischaemic heart. *Nature.* 2008;451:578–582.
- Morand EF, Leech M, Bernhagen J. MIF: a new cytokine link between rheumatoid arthritis and atherosclerosis. *Nat Rev Drug Discov.* 2006;5:399–410.
- Pan JH, Sukhova GK, Yang JT, Wang B, Xie T, Fu H, Zhang Y, Satoskar AR, David JR, Metz CN, Bucala R, Fang K, Simon DI, Chapman HA, Libby P, Shi GP. Macrophage migration inhibitory factor deficiency impairs atherosclerosis in low-density lipoprotein receptor-deficient mice. *Circulation.* 2004;109:3149–3153.
- Baugh JA, Bucala R. Macrophage migration inhibitory factor. *Crit Care Med.* 2002;30:S27–S35.
- Bernhagen J, Krohn R, Lue H, Gregory JL, Zernecke A, Koenen RR, Dewor M, Georgiev I, Schober A, Leng L, Kooistra T, Fingerle-Rowson G, Ghezzi P, Kleemann R, McColl SR, Bucala R, Hickey MJ, Weber C. MIF is a noncognate ligand of CXC chemokine receptors in inflammatory and atherogenic cell recruitment. *Nat Med.* 2007;13:587–596.
- Merat S, Casanada F, Sutphin M, Palinski W, Reaven PD. Western-type diets induce insulin resistance and hyperinsulinemia in LDL receptor-deficient mice but do not increase aortic atherosclerosis compared with normoinsulinemic mice in which similar plasma cholesterol levels are achieved by a fructose-rich diet. *Arterioscler Thromb Vasc Biol.* 1999;19:1223–1230.
- Fingerle-Rowson G, Petrenko O, Metz CN, Forsthuber TG, Mitchell R, Huss R, Moll U, Muller W, Bucala R. The p53-dependent effects of macrophage migration inhibitory factor revealed by gene targeting. *Proc Natl Acad Sci U S A.* 2003;100:9354–9359.
- Kleemann R, Verschuren L, De Rooij BJ, Lindeman J, De Maat MM, Szalai AJ, Princen HM, Kooistra T. Evidence for anti-inflammatory activity of statins and PPARalpha activators in human C-reactive protein transgenic mice in vivo and in cultured human hepatocytes in vitro. *Blood.* 2004;103:4188–4194.
- Verschuren L, Kleemann R, Offerman EH, Szalai AJ, Emeis SJ, Princen HM, Kooistra T. Effect of low dose atorvastatin versus diet-induced cholesterol lowering on atherosclerotic lesion progression and inflammation in apolipoprotein E\*3-Leiden transgenic mice. *Arterioscler Thromb Vasc Biol.* 2005;25:161–167.
- Kleemann R, Kapurniotu A, Frank RW, Gessner A, Mischke R, Flieger O, Juttner S, Brunner H, Bernhagen J. Disulfide analysis reveals a role for macrophage migration inhibitory factor (MIF) as thiol-protein oxidoreductase. *J Mol Biol.* 1998;280:85–102.
- Kleemann R, Rorsman H, Rosengren E, Mischke R, Mai NT, Bernhagen J. Dissection of the enzymatic and immunologic functions of macrophage migration inhibitory factor. Full immunologic activity of N-terminally truncated mutants. *Eur J Biochem.* 2000;267:7183–7193.
- Atsumi T, Cho YR, Leng L, McDonald C, Yu T, Danton C, Hong EG, Mitchell RA, Metz C, Niwa H, Takeuchi J, Onodera S, Umino T, Yoshioka N, Koike T, Kim JK, Bucala R. The proinflammatory cytokine macrophage migration inhibitory factor regulates glucose metabolism during systemic inflammation. *J Immunol.* 2007;179:5399–5406.
- Hotamisligil GS. Inflammation and metabolic disorders. *Nature.* 2006;444:860–867.
- Kleemann R, Zadelaar S, Kooistra T. Cytokines and atherosclerosis: a comprehensive review of studies in mice. *Cardiovasc Res.* 2008;79:360–376.
- Weisberg SP, Hunter D, Huber R, Lemieux J, Slaymaker S, Vaddi K, Charo I, Leibel RL, Ferrante AW Jr. CCR2 modulates inflammatory and metabolic effects of high-fat feeding. *J Clin Invest.* 2006;116:115–124.
- Herder C, Kolb H, Koenig W, Haastert B, Muller-Scholze S, Rathmann W, Holle R, Thorand B, Wichmann HE. Association of systemic concentrations of macrophage migration inhibitory factor with impaired glucose tolerance and type 2 diabetes: results from the Cooperative Health Research in the Region of Augsburg, Survey 4 (KORA S4). *Diabetes Care.* 2006;29:368–371.
- Herder C, Klopp N, Baumert J, Muller M, Khuseynova N, Meisinger C, Martin S, Illig T, Koenig W, Thorand B. Effect of macrophage migration inhibitory factor (MIF) gene variants and MIF serum concentrations on the risk of type 2 diabetes: results from the MONICA/KORA Augsburg Case-Cohort Study, 1984–2002. *Diabetologia.* 2008;51:276–284.
- Kleemann R, Gervois PP, Verschuren L, Staels B, Princen HM, Kooistra T. Fibrates down-regulate IL-1-stimulated C-reactive protein gene expression in hepatocytes by reducing nuclear p50-NFkappa B-C/EBP-beta complex formation. *Blood.* 2003;101:545–551.
- Burger-Kentischer A, Gobel H, Kleemann R, Zernecke A, Bucala R, Leng L, Finkelmeier D, Geiger G, Schaefer HE, Schober A, Weber C, Brunner H, Rutten H, Ihling C, Bernhagen J. Reduction of the aortic inflammatory response in spontaneous atherosclerosis by blockade of macrophage migration inhibitory factor (MIF). *Atherosclerosis.* 2006;184:28–38.
- Carter AM. Inflammation, thrombosis and acute coronary syndromes. *Diab Vasc Dis Res.* 2005;2:113–121.

## **Supplement Material**

### **Extended Materials and Methods**

#### **Analyses in plasma**

Total plasma cholesterol and triglyceride levels were measured after 4 h of fasting, using kits No. 11489437 and 11488872 (Roche Diagnostics, Almere, The Netherlands), respectively.<sup>1</sup> For lipoprotein profiles, pooled plasma was fractionated using an ÅKTA FPLC system (Pharmacia, Roosendaal, The Netherlands).<sup>2</sup> Serum amyloid A (SAA) and fibrinogen were determined by ELISA as reported<sup>1,3</sup>. Adiponectin, leptin, E-selectin, and VCAM-1 were quantified by established ELISAs (R&D Systems Europe, Ltd., Abingdon, United Kingdom). Plasma glucose was measured using the glucose hexokinase method (Instruchemie, Delfzijl, The Netherlands) and plasma insulin concentrations were determined by ELISA (Mercordia AB, Sweden). Homeostasis model assessment (HOMA) index was calculated according to the formula  $HOMA = \text{fasting plasma glucose (mM)} \times \text{fasting plasma insulin (ng/mL)} / 22.5$ .

#### **Analyses in computerized metabolic cages**

Groups of n=8 male mice per genotype were subjected to individual indirect calorimetry measurements for a period of 3 consecutive days (Comprehensive Laboratory Animal Monitoring System, Columbus Instruments, Columbus Ohio, USA) essentially as reported<sup>4</sup>. A period of 24 h was included before the start of the experiment to allow acclimatization of the animals to the cages and to the single housing. Experimental analysis started at 6 p.m. and continued for 50 h. Animals were fed a chow diet. Analyzed parameters included real time food and water intake, as well as meal size, frequency and

duration. Individual measurements of oxygen consumption ( $\text{VO}_2$ ) and carbon dioxide production rates ( $\text{VCO}_2$ ) were performed at intervals of 14 min. Respiratory exchange rate (RER) as a measure for metabolic substrate choice was calculated using the formula:  $\text{RER} = \text{VCO}_2/\text{VO}_2$ . Activity was monitored as infrared beam breaks in both X and Y axis.

### **Glucose and insulin tolerance tests**

Glucose and insulin tolerance tests were based on the protocols described by Merat<sup>5</sup> and Solinas<sup>6</sup>. After a 4 h-fast, mice were intraperitoneally injected with glucose (2 g/kg body weight). Blood samples were taken at various time points (0–120 min), and blood glucose was determined with a glucose analyzer (FreeStyle; Disetronics, Vianen, The Netherlands). For insulin tolerance tests (IST), 4 h-fasted mice were intraperitoneally treated with human insulin (0.5 U /25 g body weight). Blood samples were taken at regular time points (0–90 min) to measure glucose by ELISA. The experimental conditions for IST were pathologic conditions for old (>35 w) animals.

### **Hyperinsulinemic-euglycemic clamp analysis**

The clamp experiments were performed as described<sup>7</sup>. Briefly, after an overnight fast, animals were anesthetized (0.5 mL/kg Hypnorm; Janssen Pharmaceutica, Berchem, Belgium and 12.5 mg/g midazolam; Genthon BV, Nijmegen, The Netherlands) and an infusion needle was placed in one of the tail veins. Subsequently, a bolus of insulin (200 mU/kg; Actrapid, Novo Nordisk, Chartres, France) was given, and a hyperinsulinemic-euglycemic clamp was started with a continuous infusion of insulin (3.5 mU/min·kg) and a variable infusion of 12.5% D-glucose (in phosphate-buffered saline [PBS]) to maintain

blood glucose level at euglycemic levels of 7.5 mmol/L. Blood samples were taken every 5 to 10 min and plasma glucose levels were monitored using a hand-glucose meter (FreeStyle; Disetronics, Vianen, The Netherlands). Glucose infusion rates were calculated as described <sup>7</sup>. The experimental conditions for clamp analysis were pathologic conditions for old (>35 w) animals.

### **Western Blotting and co-immunoprecipitation**

All tissue extracts were prepared in the presence of proteinase inhibitors (PI) (Roche Diagnostics). Western blotting experiments were performed using anti-MIF antibodies (sc-2012; sc-16965) and an anti- $\beta$ -actin (sc-1615) control antibody as reported previously.<sup>8</sup> Primary and secondary antibodies were obtained from Santa Cruz Biotechnology (Heerhugowaard, The Netherlands). Immunoblots were visualized using the Super Signal West Dura Extended Duration Substrate (Pierce, St Augustin, Germany) and analyzed using a luminescent image workstation (Roche Diagnostics).

### **Insulin signaling**

Tissue biopsies were homogenized in phosphoinositide-3-kinase (PI3K) lysis buffer using an Ultraturrax mixer as reported previously <sup>9</sup>. Protein content was determined using the BCA kit (Pierce, Rockford, IL, USA). For PI3K activity analysis, Insulin Receptor Substrate 1 (IRS1) was immunoprecipitated overnight (4°C) from 2 mg protein using IRS1 antibody K6 <sup>9</sup>, and the associated kinase activity was determined essentially as described <sup>10</sup>. AKT phosphorylation in tissue homogenates was analyzed by Western blotting using phospho-specific AKT-Ser473 antibody (Cell Signaling Technology, Beverly, MA, USA)<sup>11</sup>.

### **Nucleic acid extraction and microarray analysis**

Total RNA was extracted from epididymal adipose tissue using RNazol (Campro Scientific, Veenendaal, The Netherlands) and glass beads according to the manufacturer's instructions. The integrity of the isolated RNA was examined by Agilent Lab-on-a-chip technology using the RNA 6000 Nano LabChip kit and a Bioanalyzer 2100 (both Agilent Technologies, Amstelveen, The Netherlands)<sup>3</sup>. A One-Cycle Target Labeling and Control Reagent kit (Affymetrix #900493) was used to prepare biotinylated cRNA (from 5 µg of total RNA; n=3) for microarray hybridization following the protocols of the manufacturer (Affymetrix). The quality of biotin-labeled cRNA and fragmented cRNA was again controlled using the RNA 6000 Nano Lab-on-a-chip and Bioanalyzer 2100. Microarray analysis was carried out using Affymetrix GeneChip® mouse full genome 430 2.0 arrays (45,037 probe sets; 34,000 mouse genes). Briefly, fragmented cRNA was mixed with spiked controls, tested on Affymetrix Test Chips®, and then hybridized with murine GeneChip® 430 2.0 arrays<sup>3</sup>. The protocols for hybridization, probe array washing and staining were executed as described by Affymetrix, and probe arrays were scanned with a Hewlett-Packard Gene Array Scanner (Leiden Genome Technology Center, Leiden, The Netherlands).

For parallel quantitative real-time polymerase chain reaction (qRT-PCR) analysis, a published procedure<sup>12</sup> was followed: a mastermix (Eurogentec, Seraing, Belgium), an ABI-7700 system (PE Biosystems, Nieuwekerk a/d IJssel, The Netherlands) and established primer/probe sets were used with cyclophilin A (PE Biosystems) as a reference.

## **Gene expression data analysis**

Microarray data analysis was carried out essentially as recently described by us<sup>3</sup>. In brief, raw signal intensities were normalized using the GCRMA algorithm (Affy package in R). Datasets are freely accessible online through ArrayExpress (<http://www.ebi.ac.uk/arrayexpress>; accession number: E-TABM-524; Reviewer's login account: Username: Reviewer\_E-TABM-524; Password: 1217407408706). Gene expression data was analyzed using GeneSpring GX7.3 (Agilent Technologies, USA). Differentially expressed genes were identified by statistical *t*-test analysis ( $P < 0.01$ ) and the criteria that a gene has to be more than 2-fold up-/down-regulated in at least two animals of the *Ldlr*<sup>-/-</sup> group when compared to its median expression in the *Mif*<sup>-/-</sup> *Ldlr*<sup>-/-</sup> group. Differentially expressed genes as well as genes with comparable expression level according to microarray analysis were verified by an independent method (RT-PCR). The differences in gene expression found by microarray analysis could be confirmed which is in line with a previous head-to-head comparison of the used microarray technology with RT-PCR.<sup>3</sup> For biological interpretation of the identified differentially expressed genes (see gene list in Online Table II), a gene enrichment analysis on gene ontology processes predefined in MetaCore™ software (GeneGo Inc., USA) was performed.

## **Immunohistochemical analysis of adipose tissue**

Directly after sacrifice, adipose tissues were fixed in formalin and embedded in paraffin to prepare cross sections (5 μm thick) for immunohistological analysis. For specific immunostaining of macrophages, c-jun, CD44 and ICAM, antibodies MAC-3 (BD Biosciences Pharmingen), sc-45, sc-18849 (both Santa Cruz Biotechnology) and GTX76543 (Genetex) were used, respectively. Biotin- (Jackson ImmunoResearch) and

Alexa Fluor488- (Invitrogen) labeled secondary antibodies were used for immunofluorescence analysis <sup>1</sup>. Stained cross-sections were covered in malinol or Vectashield with DAPI (Vector Laboratories) as mounting medium. Computer-assisted morphometric analysis was carried out on an Olympus BX51 microscope and CELL<sup>^</sup>D software (Olympus, Zoeterwoude, The Netherlands). A custom-made module within the CELL<sup>^</sup>D software was developed for the analysis of adipocyte size (the size of the area analyzed was identical for Ldlr<sup>-/-</sup> and Mif<sup>-/-</sup>Ldlr<sup>-/-</sup>) and partially photographed adipocytes were not taken into account. For the quantitative analysis of macrophage content and adhesion molecule expression in adipose tissue, areas of 880  $\mu\text{m}$  x 660  $\mu\text{m}$  were evaluated in at least 10 cross-sections per group.

### **Analyses of atherosclerosis**

Total aortic plaque load was determined in longitudinally opened Oil red O-stained aortas following a reported procedure <sup>1</sup>. To analyze atherosclerosis in the aortic valve area (aortic root), hearts were fixed and embedded in paraffin. Serial cross-sections (5  $\mu\text{m}$  thick) were prepared throughout the entire aortic valve area and stained with hematoxylin-phloxine-saffron. Atherosclerosis was analyzed blindly in 4 cross-sections of each specimen (at intervals of 30  $\mu\text{m}$ ) using QWin-software (Leica) for morphometric computer-assisted quantification of lesion area <sup>1</sup>. Monocytes and macrophages were immunostained in cross-sections adjacent to those used for quantification of atherosclerosis using AIA31240 (1:3000, Accurate Chemical and Scientific, Brussels, Belgium). The number of monocytes lumenally attached to the endothelium were counted and the macrophage-containing lesion area was quantified (QWin-software).

## Statistical analysis

Differences between two sets of data were compared by Student's *t* test, and differences over time were compared by two-way analysis of variance (ANOVA) using SPSS 11.5 for Windows (SPSS, Chicago, USA). Differences were considered significant at  $P < 0.05$ .

## References

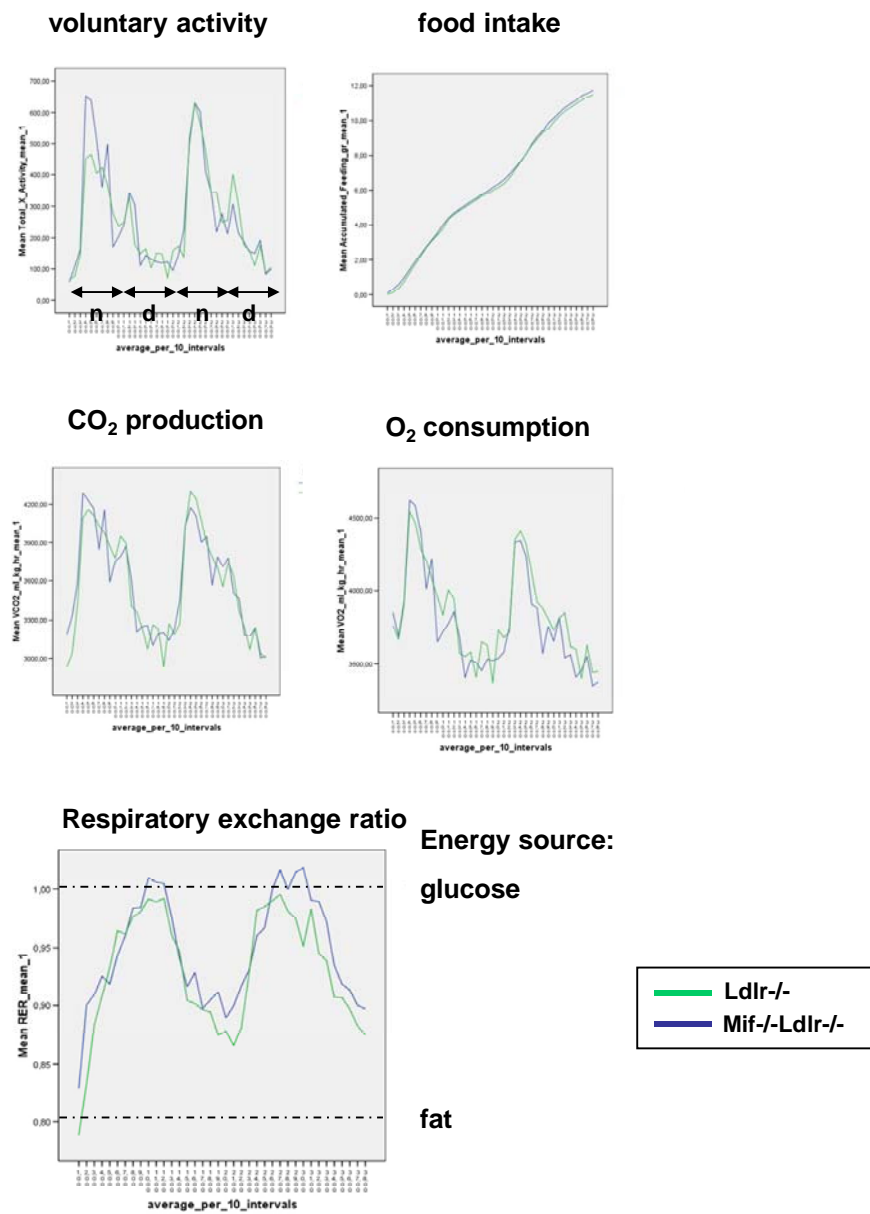
1. Verschuren L, Kleemann R, Offerman EH, Szalai AJ, Emeis SJ, Princen HM, Kooistra T. Effect of low dose atorvastatin versus diet-induced cholesterol lowering on atherosclerotic lesion progression and inflammation in apolipoprotein E\*3-Leiden transgenic mice. *Arterioscler Thromb Vasc Biol.* 2005;25:161-167.
2. Rein D, Schijlen E, Kooistra T, Herbers K, Verschuren L, Hall R, Sonnewald U, Bovy A, Kleemann R. Transgenic flavonoid tomato intake reduces C-reactive protein in human C-reactive protein transgenic mice more than wild-type tomato. *J Nutr.* 2006;136:2331-2337.
3. Kleemann R, Verschuren L, van Erk MJ, Nikolsky Y, Cnubben NH, Verheij ER, Smilde AK, Hendriks HF, Zadelaar S, Smith GJ, Kaznacheev V, Nikolskaya T, Melnikov A, Hurt-Camejo E, van der GJ, van OB, Kooistra T. Atherosclerosis and liver inflammation induced by increased dietary cholesterol intake: a combined transcriptomics and metabolomics analysis. *Genome Biol.* 2007;8:R200.
4. Madsen L, Pedersen LM, Liaset B, Ma T, Petersen RK, van den BS, Pan J, Muller-Decker K, Dulsner ED, Kleemann R, Kooistra T, Dorskeland SO, Kristiansen K. cAMP-dependent signaling regulates the adipogenic effect of n-6 polyunsaturated fatty acids. *J Biol Chem.* 2008;283:7196-7205.
5. Merat S, Casanada F, Sutphin M, Palinski W, Reaven PD. Western-type diets induce insulin resistance and hyperinsulinemia in LDL receptor-deficient mice but do not increase aortic atherosclerosis compared with normoinsulinemic mice in which similar plasma cholesterol levels are achieved by a fructose-rich diet. *Arterioscler Thromb Vasc Biol.* 1999;19:1223-1230.
6. Solinas G, Vilcu C, Neels JG, Bandyopadhyay GK, Luo JL, Naugler W, Grivennikov S, Wynshaw-Boris A, Scadeng M, Olefsky JM, Karin M. JNK1 in hematopoietically derived cells contributes to diet-induced inflammation and insulin resistance without affecting obesity. *Cell Metab.* 2007;6:386-397.
7. Voshol PJ, Jong MC, Dahlmans VE, Kratky D, Levak-Frank S, Zechner R, Romijn JA, Havekes LM. In muscle-specific lipoprotein lipase-overexpressing mice,

muscle triglyceride content is increased without inhibition of insulin-stimulated whole-body and muscle-specific glucose uptake. *Diabetes*. 2001;50:2585-2590.

8. Kleemann R, Gervois PP, Verschuren L, Staels B, Princen HM, Kooistra T. Fibrates down-regulate IL-1-stimulated C-reactive protein gene expression in hepatocytes by reducing nuclear p50-NFkappa B-C/EBP-beta complex formation. *Blood*. 2003;101:545-551.
9. Ouwens DM, van der Zon GC, Pronk GJ, Bos JL, Moller W, Cheatham B, Kahn CR, Maassen JA. A mutant insulin receptor induces formation of a Shc-growth factor receptor bound protein 2 (Grb2) complex and p21ras-GTP without detectable interaction of insulin receptor substrate 1 (IRS1) with Grb2. Evidence for IRS1-independent p21ras-GTP formation. *J Biol Chem*. 1994;269:33116-33122.
10. Burgering BM, Medema RH, Maassen JA, van de Wetering ML, van der Eb AJ, McCormick F, Bos JL. Insulin stimulation of gene expression mediated by p21ras activation. *EMBO J*. 1991;10:1103-1109.
11. Ouwens DM, Boer C, Fodor M, de GP, Heine RJ, Maassen JA, Diamant M. Cardiac dysfunction induced by high-fat diet is associated with altered myocardial insulin signalling in rats. *Diabetologia*. 2005;48:1229-1237.
12. Kooistra T, Verschuren L, de Vries-van der Weij, Koenig W, Toet K, Princen HM, Kleemann R. Fenofibrate reduces atherogenesis in ApoE\*3Leiden mice: evidence for multiple antiatherogenic effects besides lowering plasma cholesterol. *Arterioscler Thromb Vasc Biol*. 2006;26:2322-2330.

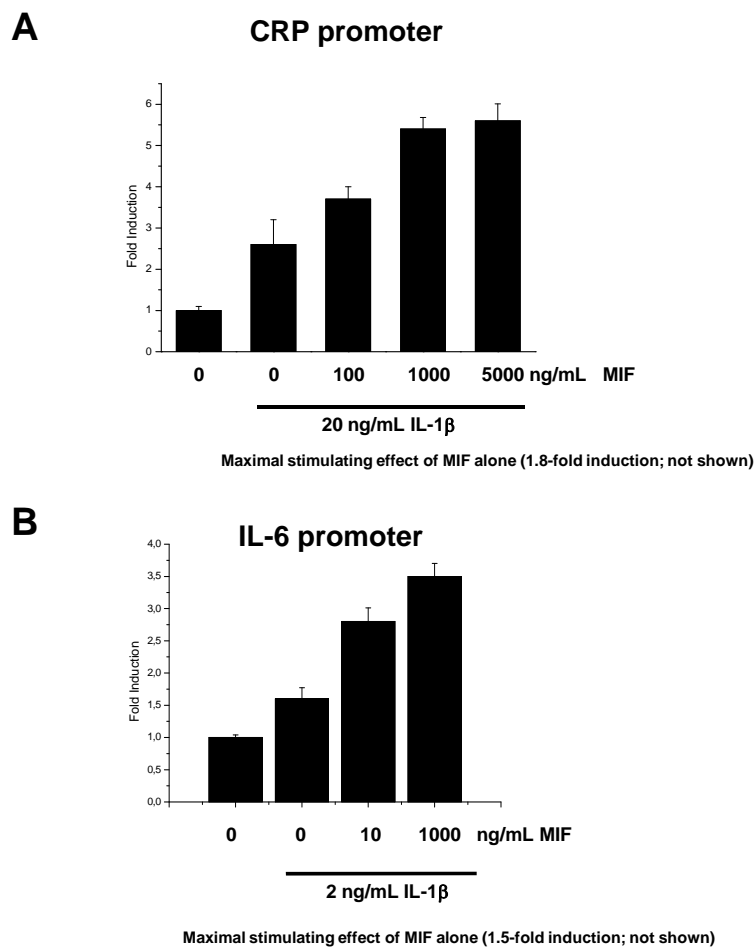
## Online Figure I

**Effect of MIF-deficiency on metabolic performance.** Groups of n=8 animals (Ldlr<sup>-/-</sup>, green; Mif<sup>-/-</sup>Ldlr<sup>-/-</sup>, blue) were monitored in computerized metabolic cages.



## Online Figure II

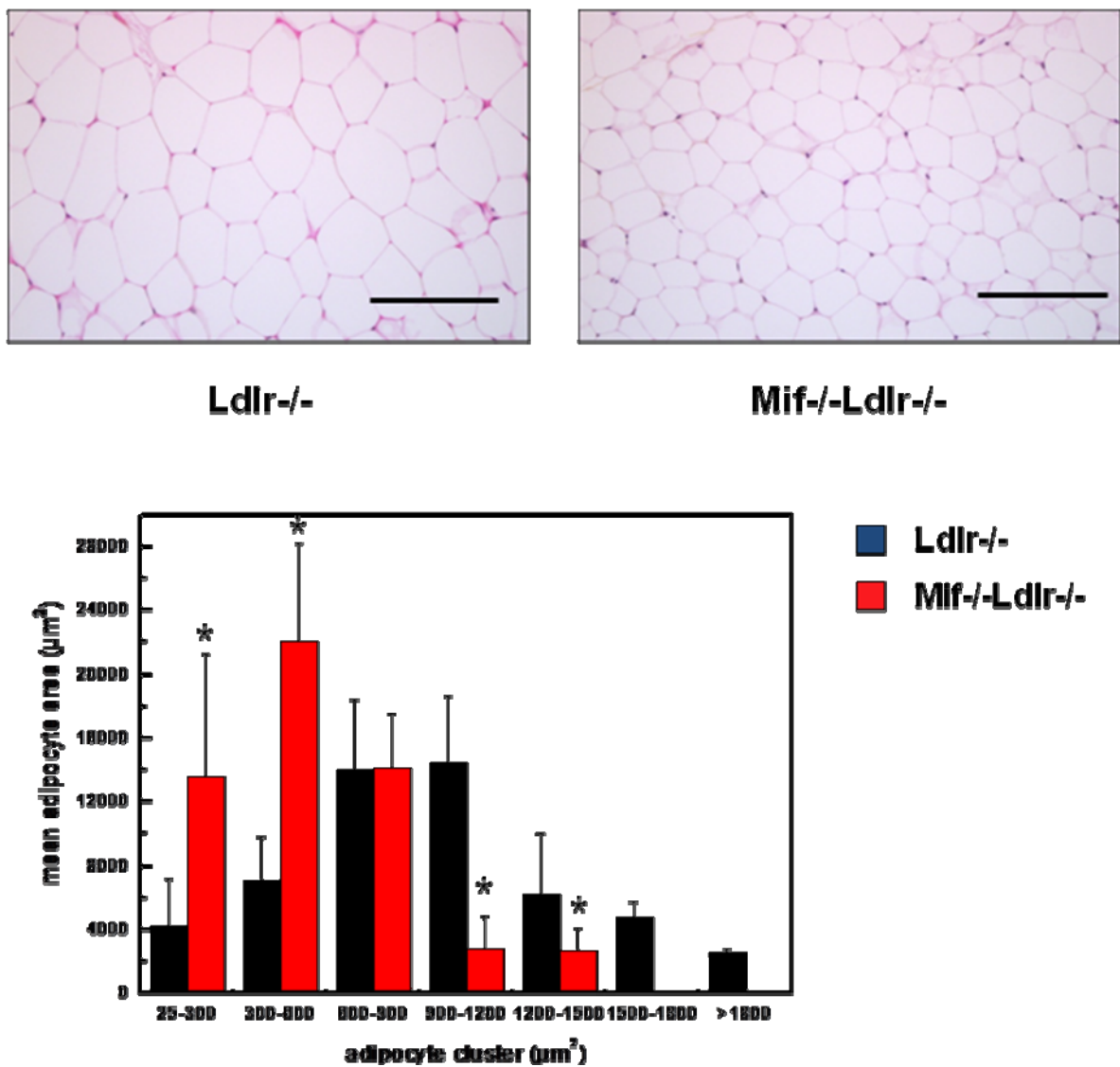
**MIF activates the human CRP and human IL-6 promoter.** HuH7 hepatoma cells ( $1.2 \times 10^5$ ) were transiently transfected with 100 ng of a luciferase reporter plasmid carrying a 300-bp fragment of (A) the human CRP promoter or (B) the IL-6 promoter using the FUGENE6 transfection reagent (Roche Diagnostics). Cells were stimulated with cytokines and harvested after 18 h. Reporter gene activity was determined using the dual-luciferase reporter assay system (Promega). A renilla luciferase constructed was co-transfected to correct for differences in transfection efficiency.



### Online Figure III

#### Effect of MIF-deficiency on adipocyte size in WAT of young (12-18 w old) animals.

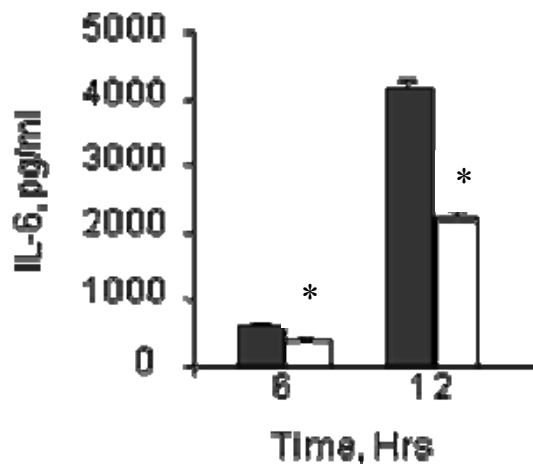
Representative photomicrographs and computerized quantification of adipocyte size in *Ldlr*<sup>-/-</sup> (black bars) and *Mif*<sup>-/-</sup>*Ldlr*<sup>-/-</sup> (red bars) mice at 15 w of age, i.e. prior to macrophage infiltration in *Ldlr*<sup>-/-</sup>. Data shown are absolute values and expressed as means  $\pm$  SD ( $n \geq 5$ ). Significant difference between groups is indicated \* $P < 0.05$ .



## Online Figure IV

### Effect of MIF-deficiency on the inflammatory responsiveness of macrophages.

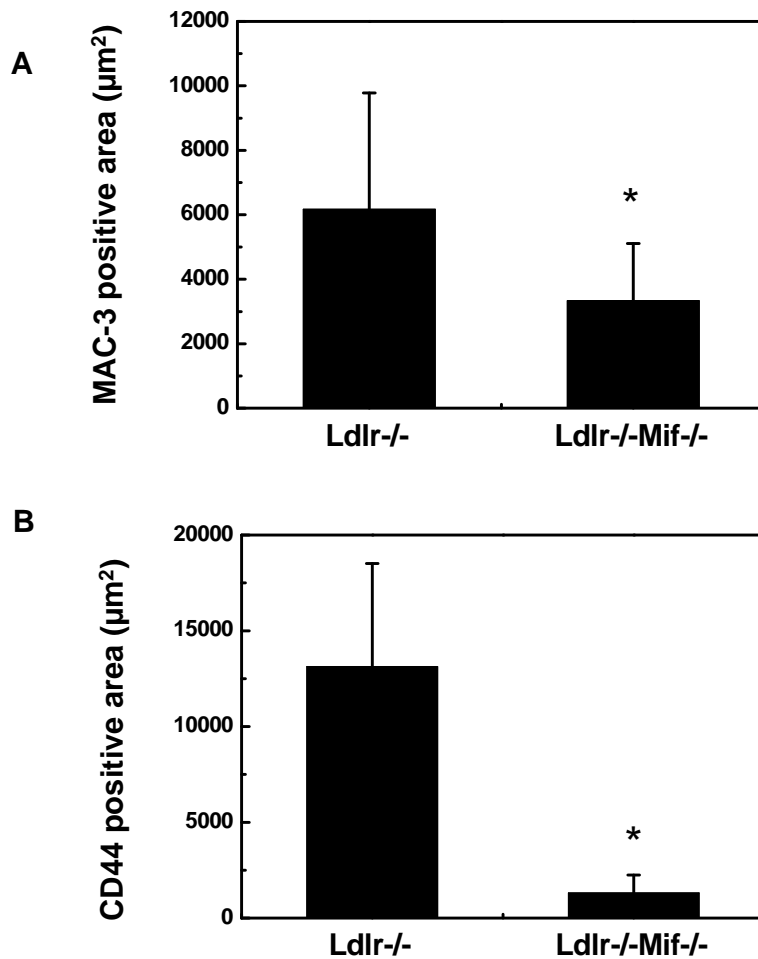
Thioglycollate-elicited macrophages were isolated from wild-type mice (black bars) and MIF<sup>-/-</sup> mice (white bars). Cells were stimulated with LPS. Supernatants were harvested after 6 h and 12 h, and assayed for IL-6 by ELISA. \*P<0.05.



## Online Figure V

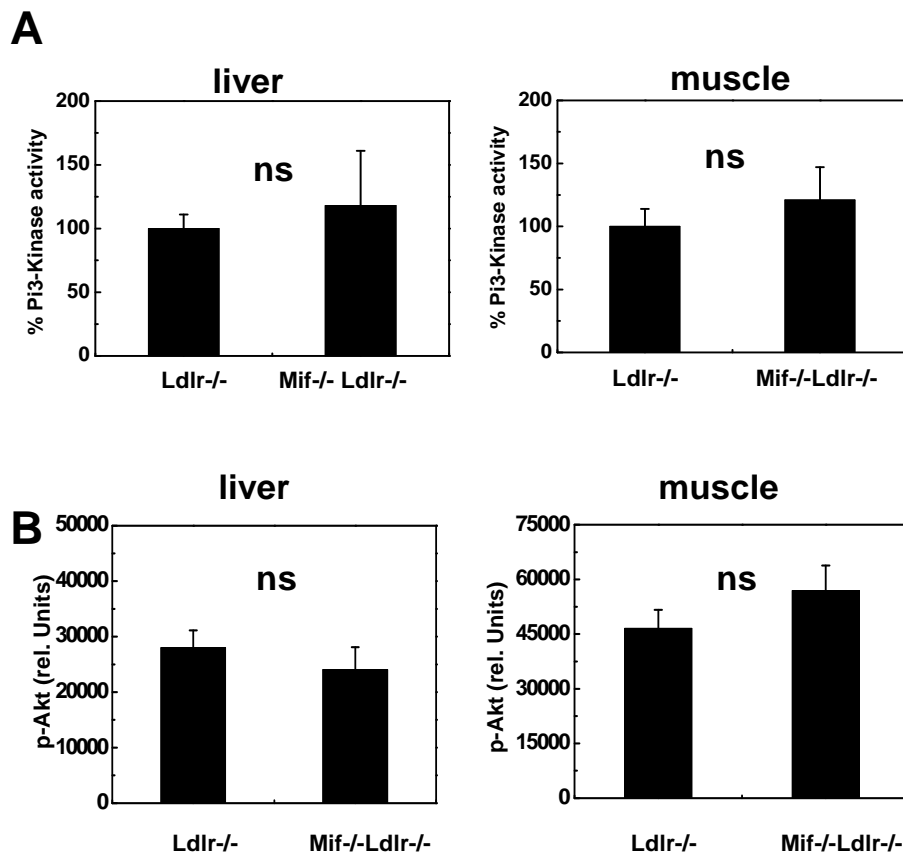
### Effect of MIF-deficiency on macrophage area and CD44 expression in WAT.

Computer-assisted (QWin software; Leica) quantification of the MAC3-positive area and the CD44-positive area in cross-sections prepared from WAT of Ldlr<sup>-/-</sup> and Mif<sup>-/-</sup> Ldlr<sup>-/-</sup> mice. \*P<0.05 indicates significant differences.



## Online Figure VI

**Effect of MIF-deficiency on PI3-kinase and p-AKT in liver and muscle.** PI3-kinase activity and p-AKT levels in liver and muscle. Ldlr<sup>-/-</sup> and Ldlr<sup>-/-</sup>Mif<sup>-/-</sup> mice (n=7 each) were sacrificed precisely 10 min after treatment with 0.5 U insulin per 25 g body weight. Data are means  $\pm$  SD. Significant differences are indicated \*P<0.05.



## Online Table I

**Overview of pathways in epididymal adipose tissue that are affected in Ldlr<sup>-/-</sup> as compared to Mif<sup>-/-</sup>Ldlr<sup>-/-</sup>.** Differentially expressed genes were analyzed across pathways using MetaCore™ and according to standard Gene Ontology (GO) Biological Process nomenclature. Categories, processes and genes are listed including their *P*-value.

<b>Processes affected by Mif in epididymal adipose tissue</b>		
<b>Biological category</b>	<b>Functional process</b>	<b><i>P</i>-value</b>
Cell signaling	IGF-R1 signalling [Igfbp2, Igfbp6, Gsk3b, Ywhaz]	0.040
	leptin signalling via JAK/STAT and MAPK cascades [Map2k1, Pla2g4a, Egr1]	0.043
	Insulin receptor pathway signalling [Gsk3b, Map2k1, Fasd2]	0.100
	Signaling through ASK1 [Sod1, Rrm2, Gsk3b, Hsp90aa1, Hspa1a, Hspa1b]	0.001
	Signaling pathway mediated by IL-6 and IL-1 [Il6st, Irak2]	0.067
Cell cycle control	Nucleocytoplasmic transport of CDK/cyclins [Gsk3b, Ccna2, Cdc2]	0.018
	ATM/ATR regulation of G2/M checkpoint [Atm, Ccna2, Cdc2]	0.036
	Cell cycle regulation by 14-3-3 proteins [Ywhaz, Cdc2, Atm]	0.030
Immune response	MIF in innate immunity response [Mif, Irak2]	0.062
	ERK interactions [Dusp3, Camk2b, Map2k1, Prkd2]	0.062
	Integrin-mediated cell adhesion [Col4a2, Itga7, Actn1, Mylk, Myh11, Myh9]	0.097
	IL-3 activation and signaling [Csf2rb, Map2k1, Egr1]	0.067
(Lipid) metabolism	Cholesterol biosynthesis [Hmgcs1, Dhcr24, Dhcr7]	0.017
	PPAR regulation of lipid metabolism [Acs14, Fabp5, Cpt1a]	0.036
	Prostaglandin 1 (prostaglandin 2) biosynthesis and metabolism [Alox15, Ptgs1, Ptgis, Hpgd]	0.001 (0.017)
	Unsaturated fatty acid biosynthesis [Acs14, Fads1, Fds2]	0.044

Online Table II

Probe Set ID	Gene Title	Gene Symbol	median of ratio (Ldlr <sup>-/-</sup> ) vs (Ldlr <sup>-/-</sup> Mif <sup>-/-</sup> )	P-value
1416335_at	macrophage migration inhibitory factor	Mif	40.94	0.0001
1427247_at	DNA segment, Chr 3, Brigham & Women's Genetics 0562 expressed	968568 S06wg0562e	10.52	0.0073
1435314_at	tryptophan hydroxylase 2	Tph2	8.11	
1454608_x_at	transthyretin	Ttr	7.68	
1419473_a_at	cholecystokinin	Cck	7.22	
1455913_x_at	transthyretin	Ttr	6.81	
1425385_a_at	Immunoglobulin heavy chain complex	Igh-6	6.18	0.0033
1434437_x_at	ribonucleotide reductase M2	Rrm2	4.70	0.0110
1451801_at	triadin	Trdn	4.63	
1448664_a_at	SPEG complex locus	Speg	4.08	
1437669_x_at	Chemokine (C-C motif) receptor-like 1	Ccr1	3.71	
1448619_at	7-dehydrocholesterol reductase	Dhcr7	3.63	0.0364
1419248_at	regulator of G-protein signaling 2	Rgs2	3.40	0.0174
1415823_at	stearoyl-Coenzyme A desaturase 2	Scd2	3.36	0.0207
1454995_at	---	---	3.35	0.0077
1420699_at	C-type lectin domain family 7, member a	Clec7a	3.28	
1426817_at	antigen identified by monoclonal antibody Ki 67	Mki67	3.22	
1427363_at	---	---	3.17	
1451527_at	procollagen C-endopeptidase enhancer 2	Pcolce2	3.13	0.0319
1426143_at	triadin	Trdn	3.13	
1441206_at	synaptopodin 2	Synpo2	3.11	
1431374_at	RIKEN cDNA 6330407A03 gene	6330407A03Rik	3.11	
1417376_a_at	cell adhesion molecule 1	Cadm1	2.99	
1441915_s_at	RIKEN cDNA 2310076L09 gene	2310076L09Rik	2.96	
1425784_a_at	olfactomedin 1	Olfm1	2.94	
1436746_at	WNK lysine deficient protein kinase 1	Wnk1	2.90	
1434873_a_at	centaurin, beta 1 /// similar to Centaurin, beta 1	Centb1 /// LOC100045877	2.89	
1419247_at	regulator of G-protein signaling 2	Rgs2	2.83	0.0425
1452879_at	synaptopodin 2	Synpo2	2.81	
1450379_at	moesin	Msn	2.80	
1455505_at	GATA zinc finger domain containing 2A	Gatad2a	2.79	0.0050
1426301_at	activated leukocyte cell adhesion molecule	Alcam	2.79	
1448710_at	chemokine (C-X-C motif) receptor 4	Cxcr4	2.76	
1424981_at	neurolysin (metallopeptidase M3 family)	Nln	2.73	0.0175
1453586_at	ectonucleoside triphosphate diphosphohydrolase 1	Entpd1	2.71	
1457397_at	Kruppel-like factor 14	Klf14	2.70	
1416022_at	fatty acid binding protein 5, epidermal	Fabp5	2.69	
1450731_s_at	tumor necrosis factor receptor superfamily, member 21	Tnfrsf21	2.68	
1448024_at	natriuretic peptide receptor 3	Npr3	2.68	
1453137_at	F-box protein 30	Fbxo30	2.67	
1430151_at	nischarin	Nisch	2.67	
1455106_a_at	creatine kinase, brain	Ckb	2.64	
1416168_at	serine (or cysteine) peptidase inhibitor, clade F, member 1	Serpinf1	2.64	0.0379
1424118_a_at	SPC25, NDC80 kinetochore complex component, homolog (S. cerevisiae)	Spc25e	2.61	
1422177_at	interleukin 13 receptor, alpha 2	Il13ra2	2.61	
1448079_at	ring finger protein 166	Rnf166	2.60	
1418334_at	DBF4 homolog (S. cerevisiae)	Dbf4	2.58	
1449049_at	toll-like receptor 1	Tlr1	2.58	
1449152_at	cyclin-dependent kinase inhibitor 2B (p15, inhibits CDK4) /// similar to cyclin dependent kinase 2 inhibitor B (p14-INK4b) (p15-INK4b)	Arfip1 Arfip1 LOC100475046	2.55	
1419015_at	WNT1 inducible signaling pathway protein 2	Wisp2	2.53	
1447526_at	DNA segment, Chr 5, ERATO Doi 255, expressed	D5Erd255e	2.53	
1450634_at	ATPase, H <sup>+</sup> transporting, lysosomal V1 subunit A	Atp6v1a	2.50	
1424922_a_at	bromodomain containing 4	Brd4	2.48	

Online Table II

Probe Set ID	Gene Title	Gene Symbol	median of ratio (Ldlr <sup>-/-</sup> ) vs (Ldlr <sup>-/-</sup> Mif <sup>-/-</sup> )	P-value
1426142_a_at	triadin	Trdn	2.46	
1434003_a_at	deoxyhypusine synthase	Dhps	2.45	0.0259
1434046_at	expressed sequence AA467197	AA467197	2.45	
1435990_at	a disintegrin-like and metallopeptidase (reprolysin type) with thro	Adamts2	2.45	0.0128
1418189_s_at	metastasis associated lung adenocarcinoma transcript 1 (non-co	Malat1	2.44	
1453571_at	DEP domain containing 6	Depdc6	2.43	
1425133_s_at	RAB3A interacting protein (rabin3)-like 1	Rab3il1	2.43	
1430447_a_at	leukocyte-associated Ig-like receptor 1	Lair1	2.42	
1426936_at	predicted gene, 629242 /// cDNA sequence BC005512 /// predict	629242 /// BC00	2.41	0.0186
1448575_at	interleukin 7 receptor	Il7r	2.40	
1457528_at	solute carrier family 4, sodium bicarbonate cotransporter, membr	Slc4a7	2.40	
1416102_at	tyrosine 3-monooxygenase/tryptophan 5-monooxygenase activa	Ywhaz	2.40	
1433792_at	nuclear receptor interacting protein 2	Nrip2	2.40	
1448475_at	olfactomedin-like 3	Olfml3	2.39	
1417333_at	RAS p21 protein activator 4	Rasa4	2.38	
1437001_at	glycogen synthase kinase 3 beta	Gsk3b	2.35	
1435872_at	---	---	2.35	
1416845_at	transmembrane protein 132A	Tmem132a	2.35	
1448025_at	predicted gene, 668101 /// similar to SIRP beta 1 cell surface prc	668101 /// LOC1	2.35	
1429571_a_at	sperm acrosome associated 1	Spaca1	2.34	0.0268
1418023_at	NMDA receptor-regulated gene 1	Narg1	2.34	
1456429_at	mucosa associated lymphoid tissue lymphoma translocation gen	Malt1	2.33	
1417038_at	septin 9	sep-09	2.31	
1417910_at	cyclin A2	Ccna2	2.31	
1452058_a_at	ring finger protein 11	Rnf11	2.30	
1416664_at	cell division cycle 20 homolog (S. cerevisiae)	Cdc20	2.30	
1419097_a_at	stomatin	Stom	2.28	
1449249_at	protocadherin 7	Pcdh7	2.28	
1417065_at	early growth response 1	Egr1	2.27	
1418123_at	unc-119 homolog (C. elegans)	Unc119	2.27	0.0311
1419256_at	spectrin beta 2	Spnb2	2.27	
1460566_at	microtubule-associated protein 1 A	Mtap1a	2.27	
1448452_at	interferon regulatory factor 8	Irf8	2.27	
1450042_at	aristaless related homeobox /// similar to Arx homeoprotein	Arx /// LOC1000	2.26	
1423277_at	protein tyrosine phosphatase, receptor type, K	Ptprk	2.26	
1416052_at	phosphoribosyl pyrophosphate synthetase 1	Prps1	2.25	
1455805_x_at	coiled-coil domain containing 22	Ccdc22	2.25	
1436075_at	secreted frizzled-related sequence protein 5	Sfrp5	2.25	
1433443_a_at	3-hydroxy-3-methylglutaryl-Coenzyme A synthase 1 /// similar to	Hmgcs1 /// LOC	2.25	0.0261
1418546_a_at	Stam binding protein like 1	Stambpl1	2.25	
1451895_a_at	24-dehydrocholesterol reductase	Dhcr24	2.25	0.0297
1433768_at	palladin, cytoskeletal associated protein	Palld	2.25	0.0482
1430596_s_at	vestigial like 3 (Drosophila)	Vgll3	2.25	
1423432_at	pleckstrin homology domain interacting protein	Phip	2.25	
1456769_at	dual specificity phosphatase 3 (vaccinia virus phosphatase VH1-	Dusp3	2.24	
1458218_s_at	phosphodiesterase 7A	Pde7a	2.24	
1424051_at	collagen, type IV, alpha 2	Col4a2	2.23	
1458292_at	proteasome (prosome, macropain) subunit, alpha type 1	Psm1	2.23	0.0465
1417995_at	protein tyrosine phosphatase, non-receptor type 22 (lymphoid)	Ptpn22	2.23	0.0155
1455618_x_at	tetraspanin 33	Tspan33	2.22	
1439481_at	importin 9	Ipo9	2.22	
1416295_a_at	interleukin 2 receptor, gamma chain	Il2rg	2.22	
1416345_at	predicted gene, ENSMUSG00000045455 /// translocase of inner	ENSMUSG0000	2.22	0.0459

Online Table II

Probe Set ID	Gene Title	Gene Symbol	median of ratio	P-value
			(Ldlr <sup>-/-</sup> ) vs (Ldlr <sup>-/-</sup> Mif <sup>-/-</sup> )	
1455768_at	Niemann Pick type C2	Npc2	2.22	
1449310_at	prostaglandin E receptor 2 (subtype EP2)	Ptger2	2.21	
1447621_s_at	transmembrane protein 173	Tmem173	2.21	
1456888_at	6-phosphofructo-2-kinase/fructose-2,6-biphosphatase 4	Pfkfb4	2.21	
1455030_at	protein tyrosine phosphatase, receptor type, J	Ptprj	2.21	
1434101_at	nuclear factor I/B	Nfib	2.21	
1437308_s_at	coagulation factor II (thrombin) receptor	F2r	2.21	0.0224
1417130_s_at	angiopoietin-like 4	Angptl4	2.21	
1428156_at	guanine nucleotide binding protein (G protein), gamma 2	Gng2	2.20	0.0062
1421173_at	interferon regulatory factor 4	Irf4	2.20	
1423596_at	NIMA (never in mitosis gene a)-related expressed kinase 6	Nek6	2.19	
1417586_at	timeless homolog (Drosophila)	Timeless	2.19	0.0301
1439012_a_at	deoxycytidine kinase	Dck	2.19	
1452077_at	DEAD (Asp-Glu-Ala-Asp) box polypeptide 3, Y-linked	Ddx3y	2.18	
1443037_at	---	---	2.17	
1425227_a_at	ATPase, H+ transporting, lysosomal V0 subunit A1	Atp6v0a1	2.17	
1453593_at	vestigial like 3 (Drosophila)	Vgll3	2.16	
1448404_at	secretory carrier membrane protein 2	Scamp2	2.16	
1449277_at	predicted gene, 100039053 /// chemokine (C-C motif) ligand 19 / 100039053 /// Cc		2.16	0.0236
1455299_at	vestigial like 3 (Drosophila)	Vgll3	2.16	
1428130_at	lectin, mannose-binding, 1	Lman1	2.15	
1422562_at	Ras-related associated with diabetes	Rrad	2.15	
1423774_a_at	protein regulator of cytokinesis 1	Prc1	2.15	
1418191_at	similar to ubiquitin specific protease UBP43 /// ubiquitin specific protease 1	LOC100048346	2.15	0.0192
1449419_at	dedicator of cytokinesis 8	Dock8	2.14	
1437303_at	interleukin 6 signal transducer	Il6st	2.14	
1436507_at	interleukin-1 receptor-associated kinase 2	Irak2	2.14	0.0083
1457588_at	expressed sequence C76213	C76213	2.14	
1417667_a_at	phosphotriesterase related	Pter	2.14	
1428345_at	phosphatidic acid phosphatase type 2 domain containing 2	Ppapdc2	2.14	
1434955_at	membrane-associated ring finger (C3HC4) 1	mrt-01	2.14	
1434944_at	dystrophia myotonica-protein kinase	Dmpk	2.13	
1421228_at	chemokine (C-C motif) ligand 7	Ccl7	2.13	
1416467_at	DEAD/H (Asp-Glu-Ala-Asp/His) box polypeptide 3, X-linked	Ddx3x	2.13	
1446481_at	---	---	2.13	
1424131_at	collagen, type VI, alpha 3	Col6a3	2.13	
1435903_at	CD300A antigen	Cd300a	2.13	
1434219_at	stromal interaction molecule 2	Stim2	2.13	
1460314_s_at	histone cluster 1, H3a /// histone cluster 1, H3b /// histone cluster 1, H3c /// histone cluster 1, H3d	Hist1h3a /// Hist1h3b /// Hist1h3c /// Hist1h3d	2.13	0.0019
1439825_at	deltex 3-like (Drosophila)	Dtx3l	2.13	
1442445_at	RIKEN cDNA 2610027H17 gene	2610027H17Rik	2.13	
1426528_at	neuropilin 2 /// par-3 partitioning defective 3 homolog B (C. elegans) /// neuropilin 2	Nrp2 /// Pard3b	2.13	
1450843_a_at	serine (or cysteine) peptidase inhibitor, clade H, member 1	Serpinh1	2.12	
1424130_a_at	polymerase I and transcript release factor	Ptrf	2.12	
1436659_at	doublecortin-like kinase 1	Dclk1	2.12	
1429778_at	optineurin	Optn	2.11	
1416021_a_at	predicted gene, EG620603 /// fatty acid binding protein 5, epidermal	EG620603 /// Fabp5	2.11	
1434004_at	deoxyhypusine synthase	Dhps	2.10	
1418431_at	kinesin family member 5B	Kif5b	2.10	
1415822_at	stearoyl-Coenzyme A desaturase 2	Scd2	2.10	0.0403
1428541_at	RIKEN cDNA 3321401G04 gene	3321401G04Rik	2.10	
1448314_at	cell division cycle 2 homolog A (S. pombe)	Cdc2a	2.10	0.0316
1419251_at	epidermal growth factor receptor pathway substrate 15	Eps15	2.09	

Online Table II

Probe Set ID	Gene Title	Gene Symbol	median of ratio	P-value
			(Ldlr <sup>-/-</sup> ) vs (Ldlr <sup>-/-</sup> Mif <sup>-/-</sup> )	
1421205_at	ataxia telangiectasia mutated homolog (human)	Atm	2.09	
1455796_x_at	olfactomedin 1	Olfm1	2.08	0.0327
1456733_x_at	serine (or cysteine) peptidase inhibitor, clade H, member 1	Serpinh1	2.08	
1449254_at	secreted phosphoprotein 1	Spp1	2.08	
1428585_at	actinin, alpha 1	Actn1	2.08	
1421968_a_at	non imprinted in Prader-Willi/Angelman syndrome 2 homolog (hu	Nipa2	2.08	0.0387
1419599_s_at	membrane-spanning 4-domains, subfamily A, member 6D	Ms4a6d	2.08	
1420170_at	myosin, heavy polypeptide 9, non-muscle	Myh9	2.08	
1448901_at	carboxypeptidase X 1 (M14 family)	Cpxm1	2.08	
1416759_at	microtubule associated monooxygenase, calponin and LIM domai	Mical1	2.07	
1451206_s_at	cytohesin 1 interacting protein	Cytip	2.07	
1419255_at	spectrin beta 2	Spnb2	2.07	
1428004_at	RIKEN cDNA 3300001G02 gene	3300001G02Rik	2.07	
1437497_a_at	heat shock protein 90, alpha (cytosolic), class A member 1	Hsp90aa1	2.07	
1427228_at	palladin, cytoskeletal associated protein	Palld	2.07	0.0197
1423313_at	phosphodiesterase 7A	Pde7a	2.07	
1422542_at	G protein-coupled receptor 34	Gpr34	2.07	
1423182_at	tumor necrosis factor receptor superfamily, member 13b	Tnfrsf13b	2.07	
1434866_x_at	carnitine palmitoyltransferase 1a, liver	Cpt1a	2.07	
1431792_a_at	similar to serine/threonine kinase 11 interacting protein /// serine	LOC100047492	2.06	
1457248_x_at	hydroxysteroid (17-beta) dehydrogenase 7	Hsd17b7	2.06	
1447830_s_at	regulator of G-protein signaling 2	Rgs2	2.06	0.0281
1419182_at	sushi, von Willebrand factor type A, EGF and pentraxin domain c	Svep1	2.06	
1417552_at	fibroblast activation protein	Fap	2.06	
1438508_at	---	---	2.06	
1448627_s_at	PDZ binding kinase	Pbk	2.05	0.0239
1427455_x_at	predicted gene, EG628498 /// predicted gene, ENSMUSG00000	EG628498 /// EN	2.05	
1450286_at	natriuretic peptide receptor 3	Npr3	2.05	
1427974_s_at	calcium channel, voltage-dependent, L type, alpha 1D subunit	Cacna1d	2.05	
1457717_at	expressed sequence AI987986	AI987986	2.05	
1451475_at	plexin D1	Plxnd1	2.05	
1426606_at	cartilage acidic protein 1	Crtac1	2.05	
1452534_a_at	high mobility group box 2	Hmgb2	2.05	
1435644_at	SH3 and PX domains 2B	Sh3pxd2b	2.05	
1450828_at	synaptopodin 2	Synpo2	2.05	
1455428_at	RIKEN cDNA A930008G19 gene	A930008G19Rik	2.04	
1439686_at	---	---	2.04	
1440826_s_at	transmembrane protein 103	Tmem103	2.04	
1424349_a_at	lysophosphatidylglycerol acyltransferase 1	Lpgat1	2.04	
1460710_at	adenosine A2a receptor	Adora2a	2.04	
1416714_at	interferon regulatory factor 8	Irf8	2.03	
1416040_at	lipase, gastric	Lipf	2.03	
1452595_at	a disintegrin-like and metallopeptidase (reprolysin type) with thro	Adamts4	2.03	
1453012_at	TSC22 domain family, member 2	Tsc22d2	2.03	
1425381_a_at	transferrin receptor 2	Trfr2	2.03	
1429022_at	adenylate cyclase activating polypeptide 1 receptor 1	Adcyap1r1	2.02	
1451306_at	cell division cycle associated 7 like	Cdca7l	2.02	
1459992_x_at	ceroid-lipofuscinosis, neuronal 8	Cln8	2.02	
1424350_s_at	lysophosphatidylglycerol acyltransferase 1	Lpgat1	2.02	
1434748_at	cytoskeleton associated protein 2	Ckap2	2.02	
1418393_a_at	integrin alpha 7	Itga7	2.02	
1418022_at	NMDA receptor-regulated gene 1	Narg1	2.02	
1428897_at	RIKEN cDNA 2610029I01 gene	2610029I01Rik	2.02	

Online Table II

Probe Set ID	Gene Title	Gene Symbol	median of ratio	P-value
			(Ldlr <sup>-/-</sup> ) vs (Ldlr <sup>-/-</sup> Mif <sup>-/-</sup> )	
1421137_a_at	protein kinase inhibitor beta, cAMP dependent, testis specific	Pkib	2.02	
1427937_at	RIKEN cDNA 2610030H06 gene	2610030H06Rik	2.02	
1440153_at	---	---	2.02	
1425521_at	polyadenylate binding protein-interacting protein 1	Paip1	2.02	
1417379_at	IQ motif containing GTPase activating protein 1	Iqgap1	2.02	
1454764_s_at	solute carrier family 38, member 1	Slc38a1	2.01	
1440975_at	matrix-remodelling associated 7	Mxra7	2.01	0.0182
1453774_at	RIKEN cDNA 2810002O09 gene	2810002O09Rik	2.01	0.0096
1450733_at	bicaudal D homolog 2 (Drosophila)	Bicd2	2.01	
1438910_a_at	stomatin	Stom	2.01	
1456377_x_at	LIM domain containing 2	Limd2	2.01	0.0400
1425506_at	myosin, light polypeptide kinase	Mylk	2.00	
1453416_at	growth arrest-specific 2 like 3	Gas2l3	2.00	
1441094_at	alcohol dehydrogenase 6B (class V)	Adh6b	2.00	
1417676_a_at	protein tyrosine phosphatase, receptor type, O	Ptpro	2.00	
1446972_at	DNA segment, Chr 15, Wayne State University 126, expressed	D15Wsu126e	2.00	
1437716_x_at	kinesin family member 22	Kif22	1.90	0.0095
1422640_at	protocadherin beta 9	Pcdhb9	1.88	0.0016
1419532_at	interleukin 1 receptor, type II	Il1r2	1.80	0.0004
1427442_a_at	amyloid beta (A4) precursor protein	App	1.79	0.0050
1452250_a_at	collagen, type VI, alpha 2	Col6a2	1.79	0.0098
1454855_at	membrane associated guanylate kinase, WW and PDZ domain c	Magi2	1.78	0.0029
1416035_at	hypoxia inducible factor 1, alpha subunit	Hif1a	1.74	0.0091
1434333_a_at	protein kinase D2	Prkd2	1.57	0.0033
1440840_at	RIKEN cDNA D630004K10 gene	D630004K10Rik	1.53	0.0089
1420661_a_at	RIKEN cDNA 4933439F18 gene	4933439F18Rik	1.52	0.0027
1416340_a_at	mannosidase 2, alpha B1	Man2b1	1.52	0.0079
1434250_at	p21 (CDKN1A)-activated kinase 2	Pak2	1.50	0.0073
1450200_s_at	colony stimulating factor 2 receptor, beta, low-affinity (granulocyt	Csf2rb /// Csf2rb	1.50	0.0029
1436728_s_at	regulator of telomere elongation helicase 1	Rtel1	1.49	0.0023
1428081_at	kelch-like 21 (Drosophila)	Klhl21	1.47	0.0080
1430692_a_at	sel-1 suppressor of lin-12-like (C. elegans)	Sel1l	1.47	0.0085
1419838_s_at	polo-like kinase 4 (Drosophila)	Plk4	1.43	0.0080
1425185_at	RIKEN cDNA 5830417C01 gene	5830417C01Rik	1.42	0.0068
1434176_x_at	polymerase (DNA-directed), delta interacting protein 3	Poldip3	1.40	0.0078
1436707_x_at	non-SMC condensin I complex, subunit H	Ncaph	1.38	0.0058
1416351_at	mitogen-activated protein kinase kinase 1	Map2k1	1.33	0.0035
1429503_at	RIKEN cDNA 2900024C23 gene	2900024C23Rik	1.33	0.0058
1433559_at	solute carrier family 45, member 4	Slc45a4	1.27	0.0084
1433632_at	interferon regulatory factor 2 binding protein 2	Irf2bp2	1.25	0.0030
1448476_at	nucleosome assembly protein 1-like 4	Nap1l4	1.24	0.0058
1423581_at	N-myristoyltransferase 2	Nmt2	1.23	0.0015
1424426_at	methylthioadenosine phosphorylase	Mtap	1.23	0.0085
1428846_at	tetratricopeptide repeat domain 14	Ttc14	1.23	0.0066
1438232_at	forkhead box P2	Foxp2	1.22	0.0039
1455955_s_at	sorting nexin 17	Snx17	1.22	0.0074
1419135_at	lymphotoxin B	Ltb	1.21	0.0100
1418662_at	RIKEN cDNA 2210012G02 gene	2210012G02Rik	1.21	0.0011
1429887_at	RIKEN cDNA 2310005C01 gene /// nitric oxide synthase 1, neur	2310005C01Rik	1.18	0.0030
1437102_at	YTH domain family 1	Ythdf1	1.17	0.0037
1452218_at	coiled-coil domain containing 117	Ccdc117	1.01	0.0096
1423798_a_at	eukaryotic translation initiation factor 1	Eif1	0.93	0.0060
1456547_at	---	---	0.86	0.0014

Online Table II

Probe Set ID	Gene Title	Gene Symbol	median of ratio (Ldlr <sup>-/-</sup> ) vs (Ldlr <sup>-/-</sup> Mif <sup>-/-</sup> )		P-value
1418999_at	RIKEN cDNA 2310033P09 gene	2310033P09Rik	0.83	0.0071	
1457228_x_at	GLE1 RNA export mediator (yeast)	Gle1	0.83	0.0009	
1455723_at	DNA segment, Chr 1, ERATO Doi 448, expressed	D1Ert448e	0.83	0.0072	
1441263_a_at	RIKEN cDNA A930005H10 gene	A930005H10Rik	0.83	0.0037	
1448948_at	recombination activating gene 1 activating protein 1	Rag1ap1	0.82	0.0016	
1436518_at	---	---	0.82	0.0030	
1433561_at	centaurin, beta 2	Centb2	0.82	0.0066	
1434446_at	insulin receptor	Insr	0.79	0.0039	
1435346_at	coiled-coil domain containing 82	Ccdc82	0.79	0.0015	
1422792_at	platelet-activating factor acetylhydrolase, isoform 1b, alpha2 sub	Pafah1b2	0.78	0.0024	
1444766_at	ataxin 7-like 1	Atxn7l1	0.78	0.0050	
1424172_at	hydroxyacyl glutathione hydrolase	Hagh	0.77	0.0006	
1459931_a_at	---	---	0.77	0.0094	
1427906_at	RIKEN cDNA 1110037F02 gene	1110037F02Rik	0.77	0.0099	
1438477_a_at	methylmalonyl CoA epimerase	Mcee	0.76	0.0090	
1456893_at	---	---	0.75	0.0040	
1429028_at	dedicator of cytokinesis 11	Dock11	0.75	0.0080	
1426968_a_at	retinol dehydrogenase 10 (all-trans)	Rdh10	0.75	0.0095	
1458185_at	THAP domain containing 4	Thap4	0.74	0.0004	
1425824_a_at	proprotein convertase subtilisin/kexin type 4	Pcsk4	0.74	0.0072	
1427205_x_at	coiled-coil domain containing 46	Ccdc46	0.72	0.0092	
1436964_at	DNA segment, Chr 7, ERATO Doi 715, expressed	D7Ert715e	0.70	0.0059	
1416810_at	male enhanced antigen 1	Mea1	0.70	0.0078	
1450561_a_at	surfeit gene 1	Surf1	0.70	0.0048	
1455352_at	RIKEN cDNA 2610101N10 gene	2610101N10Rik	0.69	0.0012	
1424052_at	THAP domain containing 4	Thap4	0.69	0.0019	
1421479_at	zinc finger protein 318	Zfp318	0.69	0.0099	
1435860_at	solute carrier family 5 (sodium-dependent vitamin transporter), n	Slc5a6	0.69	0.0012	
1444606_at	ephrin A2	Efna2	0.68	0.0085	
1453132_a_at	gastrokine 2	Gkn2	0.68	0.0044	
1455152_at	expressed sequence AI462493	AI462493	0.68	0.0065	
1434618_at	CREB/ATF bZIP transcription factor	Crebzf	0.68	0.0044	
1429106_at	RIKEN cDNA 4921509J17 gene	4921509J17Rik	0.68	0.0079	
1446228_at	endoplasmic reticulum metalloproteinase 1	Ermp1	0.67	0.0009	
1417906_at	predicted gene, 100042114 /// RIKEN cDNA 1700001F09 gene / 100042114 /// 17		0.66	0.0081	
1456880_at	---	---	0.65	0.0010	
1436613_at	coronin, actin binding protein 6	Coro6	0.65	0.0013	
1425147_at	RIKEN cDNA 2410075B13 gene	2410075B13Rik	0.64	0.0004	
1417408_at	coagulation factor III	F3	0.64	0.0013	
1428776_at	solute carrier family 10 (sodium/bile acid cotransporter family), n	Slc10a6	0.63	0.0035	
1456121_at	centrosomal protein 97	Cep97	0.63	0.0030	
1434296_at	cDNA sequence BC049349	BC049349	0.62	0.0037	
1440894_at	transmembrane and tetratricopeptide repeat containing 3	Tmtc3	0.62	0.0025	
1455466_at	G protein-coupled receptor 133	Gpr133	0.61	0.0049	
1416939_at	pyrophosphatase (inorganic) 1	Ppa1	0.59	0.0027	
1456973_at	---	---	0.59	0.0031	
1424091_at	expressed sequence AI449175	AI449175	0.59	0.0084	
1460003_at	expressed sequence AI956758	AI956758	0.58	0.0073	
1440649_at	Predicted gene, EG232599	EG232599	0.58	0.0099	
1447147_at	---	---	0.57	0.0090	
1431377_at	ataxin 10	Atxn10	0.56	0.0006	
1444450_at	RIKEN cDNA 9530096D07 gene	9530096D07Rik	0.56	0.0067	
1451993_at	RIKEN cDNA 9130404D08 gene	9130404D08Rik	0.56	0.0053	

Online Table II

Probe Set ID	Gene Title	Gene Symbol	median of ratio	P-value
			(Ldlr <sup>-/-</sup> ) vs (Ldlr <sup>-/-</sup> Mif <sup>-/-</sup> )	
1437416_at	cDNA sequence BC034902	BC034902	0.54	0.0036
1448468_a_at	potassium voltage-gated channel, shaker-related subfamily, beta	Kcnab1	0.54	0.0088
1454388_at	RIKEN cDNA 2900046F13 gene	2900046F13Rik	0.53	0.0049
1438530_at	tissue factor pathway inhibitor	Tfpi	0.50	
1436413_at	fyn-related kinase	Frk	0.50	
1423889_at	predicted gene, EG434402	EG434402	0.50	
1452609_at	RIKEN cDNA 1190005106 gene	1190005106Rik	0.50	
1455607_at	R-spondin 3 homolog (Xenopus laevis)	Rspo3	0.50	
1441102_at	prolactin receptor	Prlr	0.50	
1449222_at	Epstein-Barr virus induced gene 3	Ebi3	0.50	
1416716_at	embryonal Fyn-associated substrate	Efs	0.49	0.0268
1417429_at	flavin containing monooxygenase 1	Fmo1	0.49	
1448989_a_at	myosin IB	Myo1b	0.49	
1442359_at	six transmembrane epithelial antigen of prostate 2	Steap2	0.49	
1459976_s_at	superoxide dismutase 1, soluble	Sod1	0.49	
1423084_at	UDP-Gal:betaGlcNAc beta 1,3-galactosyltransferase, polypeptid	B3galt2	0.49	
1421422_at	RIKEN cDNA 5033411D12 gene	5033411D12Rik	0.49	0.0352
1420688_a_at	sarcoglycan, epsilon	Sgce	0.49	
1429339_a_at	acyl-Coenzyme A dehydrogenase family, member 10	Acad10	0.49	
1426887_at	nudix (nucleoside diphosphate linked moiety X)-type motif 10 ///	Nudt10 /// Nudt1	0.49	
1425559_a_at	acyl-CoA synthetase medium-chain family member 3	Acsm3	0.49	
1448507_at	EF hand domain containing 1	Efhd1	0.48	
1424011_at	aquaporin 9	Aqp9	0.48	
1440660_at	---	---	0.48	
1428781_at	dermokine	Dmkn	0.48	
1419814_s_at	S100 calcium binding protein A1	S100a1	0.48	0.0254
1436957_at	gamma-aminobutyric acid (GABA-A) receptor, subunit alpha 3	Gabra3	0.48	
1450333_a_at	GATA binding protein 2	Gata2	0.48	
1417447_at	transcription factor 21	Tcf21	0.48	
1416200_at	interleukin 33	Il33	0.48	
1456327_at	---	---	0.48	
1436215_at	inositol polyphosphate multikinase	lpmk	0.48	
1435551_at	formin homology 2 domain containing 3	Fhod3	0.48	
1417902_at	solute carrier family 19 (thiamine transporter), member 2	Slc19a2	0.48	
1448669_at	dickkopf homolog 3 (Xenopus laevis)	Dkk3	0.48	0.0038
1434957_at	cell adhesion molecule-related/down-regulated by oncogenes	Cdon	0.48	
1429212_a_at	leucine rich repeat containing 51	Lrrc51	0.48	
1448529_at	thrombomodulin	Thbd	0.48	0.0426
1452433_at	---	---	0.48	
1437502_x_at	CD24a antigen /// predicted gene, EG621324	Cd24a /// EG621	0.48	
1433531_at	acyl-CoA synthetase long-chain family member 4	Acsl4	0.48	
1439096_at	D-aspartate oxidase	Ddo	0.48	0.0455
1416695_at	translocator protein	Tspo	0.47	
1443225_at	activin A receptor, type IC	Acvr1c	0.47	
1427932_s_at	RIKEN cDNA 1200003110 gene /// RIKEN cDNA 1200015M12 gr	1200003110Rik /	0.47	0.0049
1435767_at	sodium channel, voltage-gated, type III, beta	Scn3b	0.47	0.0058
1448034_at	expressed sequence AI842396	AI842396	0.47	0.0254
1418186_at	glutathione S-transferase, theta 1	Gstt1	0.47	
1431317_at	RIKEN cDNA 2410018L13 gene	2410018L13Rik	0.47	
1438050_x_at	predicted gene, EG668525	EG668525	0.47	
1431262_at	predicted gene, 100041195 /// predicted gene, 100041874 /// pre	100041195 /// 100041874	0.47	0.0186
1420338_at	arachidonate 15-lipoxygenase	Alox15	0.47	
1448931_at	coagulation factor II (thrombin) receptor-like 1	F2rl1	0.47	

Online Table II

Probe Set ID	Gene Title	Gene Symbol	median of ratio	P-value
			(Ldlr <sup>-/-</sup> ) vs (Ldlr <sup>-/-</sup> Mif <sup>-/-</sup> )	
1423281_at	stathmin-like 2	Stmn2	0.47	0.0145
1437867_at	---	---	0.47	
1436448_a_at	prostaglandin-endoperoxide synthase 1	Ptgs1	0.47	
1421996_at	transcription factor AP-2, alpha	Tcfap2a	0.47	
1434792_at	RIKEN cDNA 2010320M18 gene	2010320M18Rik	0.46	
1419286_s_at	intraflagellar transport 81 homolog (Chlamydomonas)	Ift81	0.46	
1422870_at	homeo box C4	Hoxc4	0.46	
1433939_at	AF4/FMR2 family, member 3	Aff3	0.46	
1449901_a_at	mitogen-activated protein kinase kinase kinase 6	Map3k6	0.46	
1459679_s_at	myosin IB	Myo1b	0.46	
1420723_at	vanin 3	Vnn3	0.46	
1426060_at	---	---	0.46	
1427183_at	epidermal growth factor-containing fibulin-like extracellular matrix protein 1	Efemp1	0.46	
1440999_at	zinc finger protein 697	Zfp697	0.46	
1438411_at	G protein-coupled receptor 81	Gpr81	0.46	
1437871_at	similar to phosphoglucomutase 5 /// phosphoglucomutase 5	LOC100046963	0.46	
1460500_at	RIKEN cDNA 5033421C21 gene	5033421C21Rik	0.46	
1435370_a_at	carboxylesterase 3	Ces3	0.46	
1439163_at	zinc finger and BTB domain containing 16	Zbtb16	0.46	0.0264
1441816_at	RIKEN cDNA 2900056M20 gene	2900056M20Rik	0.46	
1437718_x_at	fibromodulin	Fmod	0.46	
1460601_at	myosin VIIA and Rab interacting protein	Myrip	0.46	0.0463
1449918_at	CD209g antigen	Cd209g	0.45	0.0498
1435261_at	transmembrane and tetratricopeptide repeat containing 1	Tmtc1	0.45	
1420647_a_at	keratin 8	Krt8	0.45	
1429119_at	isoamyl acetate-hydrolyzing esterase 1 homolog (S. cerevisiae)	Iah1	0.45	0.0445
1437662_at	acyl-CoA synthetase medium-chain family member 5	Acsm5	0.45	0.0063
1426061_x_at	---	---	0.45	
1428636_at	six transmembrane epithelial antigen of prostate 2	Steap2	0.45	
1417434_at	glycerol phosphate dehydrogenase 2, mitochondrial	Gpd2	0.45	
1417838_at	similar to putative /// similar to putative /// hypothetical protein LC	LOC100039209	0.45	
1437433_at	UDP-Gal:betaGlcNAc beta 1,3-galactosyltransferase, polypeptide B3	galT2	0.45	
1440815_x_at	predicted gene, EG666481 /// hypothetical protein LOC624112	EG666481 /// LC	0.45	
1449081_at	carboxylesterase 3	Ces3	0.45	0.0415
1420461_at	macrophage stimulating 1 receptor (c-met-related tyrosine kinase)	Mst1r	0.45	0.0330
1456823_at	gene model 70, (NCBI)	Gm70	0.45	
1445579_at	---	---	0.44	
1438756_at	ankyrin repeat domain 29	Ankrd29	0.44	
1417421_at	S100 calcium binding protein A1	S100a1	0.44	0.0318
1435842_at	N-acetyltransferase 8-like	Nat8l	0.44	
1424713_at	calmodulin-like 4	Calml4	0.44	
1449147_at	carbohydrate (keratan sulfate Gal-6) sulfotransferase 1	Chst1	0.44	0.0325
1416055_at	RIKEN cDNA 1810008N23 gene /// amylase 2, pancreatic /// amylase 2, pancreatic	1810008N23Rik	0.44	0.0319
1456609_at	calcium/calmodulin-dependent protein kinase II inhibitor 1	Camk2n1	0.43	
1425788_a_at	enoyl Coenzyme A hydratase domain containing 2	Echdc2	0.43	
1456945_at	nudix (nucleoside diphosphate linked moiety X)-type motif 6	Nudt6	0.43	
1424790_at	solute carrier family 25, member 42	Slc25a42	0.43	0.0036
1457302_at	---	---	0.43	0.0370
1428789_at	Ral GEF with PH domain and SH3 binding motif 2	Ralgs2	0.43	
1447364_x_at	myosin IB	Myo1b	0.43	
1460259_s_at	chloride channel calcium activated 1 /// chloride channel calcium	Clca1 /// Clca2	0.43	
1416125_at	FK506 binding protein 5	Fkbp5	0.43	
1452296_at	slit homolog 3 (Drosophila)	Slit3	0.43	

Online Table II

Probe Set ID	Gene Title	Gene Symbol	median of ratio	P-value
			(Ldlr <sup>-/-</sup> ) vs (Ldlr <sup>-/-</sup> Mif <sup>-/-</sup> )	
1449325_at	fatty acid desaturase 2	Fads2	0.43	
1450850_at	ezrin /// hypothetical protein LOC100044177	Ezr /// LOC1000	0.42	
1459989_at	---	---	0.42	0.0131
1451968_at	X-ray repair complementing defective repair in Chinese hamster	Xrcc5	0.42	
1426208_x_at	pleiomorphic adenoma gene-like 1	Plagl1	0.42	
1448990_a_at	myosin IB	Myo1b	0.42	
1417867_at	complement factor D (adipsin)	Cfd	0.42	0.0454
1439760_x_at	uropod 1B	Upk1b	0.42	
1425995_s_at	Wilms tumor 1 homolog	Wt1	0.42	0.0105
1423680_at	fatty acid desaturase 1	Fads1	0.41	
1460238_at	mesothelin	Msln	0.41	
1455447_at	RIKEN cDNA D430019H16 gene	D430019H16Rik	0.41	
1419033_at	RIKEN cDNA 2610018G03 gene	2610018G03Rik	0.41	
1454890_at	angiomin	Amot	0.41	
1453588_at	carbonic anhydrase 3	Car3	0.41	
1451204_at	scavenger receptor class A, member 5 (putative)	Scara5	0.41	
1441912_x_at	complement component 2 (within H-2S)	C2	0.40	0.0412
1448816_at	prostaglandin I2 (prostacyclin) synthase	Ptgis	0.40	
1418492_at	gremlin 2 homolog, cysteine knot superfamily (Xenopus laevis)	Grem2	0.40	0.0176
1420731_a_at	cysteine and glycine-rich protein 2	Csrp2	0.40	
1456722_at	chordin-like 1	Chrdl1	0.40	0.0500
1426157_a_at	CD209b antigen	Cd209b	0.40	
1450974_at	tissue inhibitor of metalloproteinase 4	Timp4	0.40	0.0453
1452418_at	RIKEN cDNA 1200016E24 gene	1200016E24Rik	0.40	0.0230
1432358_at	mucin 16	Muc16	0.39	
1437644_at	UDP-Gal:betaGlcNAc beta 1,3-galactosyltransferase, polypeptid	B3galt2	0.38	0.0285
1453771_at	GULP, engulfment adaptor PTB domain containing 1	Gulp1	0.38	0.0093
1437685_x_at	fibromodulin	Fmod	0.38	
1436043_at	sodium channel, voltage-gated, type VII, alpha	Scn7a	0.38	
1417933_at	insulin-like growth factor binding protein 6	Igfbp6	0.38	
1418796_at	C-type lectin domain family 11, member a	Clec11a	0.38	
1423691_x_at	keratin 8	Krt8	0.38	
1436845_at	axin2	Axin2	0.37	
1415857_at	embigin	Emb	0.37	
1429379_at	lymphatic vessel endothelial hyaluronan receptor 1	Lyve1	0.36	
1437385_at	collagen and calcium binding EGF domains 1	Ccbe1	0.36	
1456084_x_at	fibromodulin	Fmod	0.36	
1434423_at	GULP, engulfment adaptor PTB domain containing 1	Gulp1	0.36	0.0026
1435399_at	synaptopodin 2	Synpo2	0.36	
1419463_at	chloride channel calcium activated 2	Clca2	0.36	
1449033_at	tumor necrosis factor receptor superfamily, member 11b (osteop	Tnfrsf11b	0.35	0.0006
1425163_at	expressed sequence AI661453	AI661453	0.35	
1427127_x_at	heat shock protein 1B	Hspa1b	0.35	
1427126_at	heat shock protein 1B	Hspa1b	0.35	
1451407_at	immunoglobulin superfamily, member 5 /// Purkinje cell protein 4	Igsf5 /// Pcp4	0.35	
1453282_at	coxsackievirus and adenovirus receptor	Cxadr	0.34	0.0100
1447886_at	RIKEN cDNA 0610040B09 gene	0610040B09Rik	0.33	
1419571_at	solute carrier family 28 (sodium-coupled nucleoside transporter),	Slc28a3	0.33	
1457664_x_at	Complement component 2 (within H-2S)	C2	0.33	0.0217
1456611_at	RIKEN cDNA D430015B01 gene	D430015B01Rik	0.33	
1436702_at	N-acetyltransferase 8-like	Nat8l	0.32	
1419905_s_at	hydroxyprostaglandin dehydrogenase 15 (NAD)	Hpgd	0.32	
1430584_s_at	carbonic anhydrase 3	Car3	0.32	

Online Table II

Probe Set ID	Gene Title	Gene Symbol	median of ratio (Ldlr <sup>-/-</sup> ) vs (Ldlr <sup>-/-</sup> Mif <sup>-/-</sup> )	P-value
1452426_x_at	---	---	0.31	
1455435_s_at	choline dehydrogenase	Chdh	0.31	
1422596_at	Na <sup>+</sup> /K <sup>+</sup> transporting ATPase interacting 4	Nkain4	0.31	
1460049_s_at	RIKEN cDNA 1500015O10 gene	1500015O10Rik	0.31	
1426183_a_at	CD209d antigen	Cd209d	0.31	
1443838_x_at	fatty acid desaturase 2	Fads2	0.31	
1425106_a_at	tryptophanyl-tRNA synthetase	Wars	0.31	
1423451_at	progesterone receptor membrane component 1	Pgrmc1	0.31	
1426934_at	NHS-like 1	Nhsl1	0.31	
1458382_a_at	---	---	0.31	
1448962_at	myosin, heavy polypeptide 11, smooth muscle	Myh11	0.31	
1423505_at	transgelin	Tagln	0.30	
1454159_a_at	insulin-like growth factor binding protein 2	Igfbp2	0.30	0.0090
1438239_at	midline 1	Mid1	0.30	
1422644_at	SH3-binding domain glutamic acid-rich protein	Sh3bgr	0.29	
1419421_at	ankyrin 1, erythroid	Ank1	0.29	
1434540_a_at	clathrin, light polypeptide (Lca)	Cltal	0.29	
1434813_x_at	tryptophanyl-tRNA synthetase	Wars	0.29	
1457065_at	uroplakin 1B	Upk1b	0.29	0.0400
1424383_at	transmembrane protein 51	Tmem51	0.29	
1435459_at	flavin containing monooxygenase 2	Fmo2	0.28	
1416034_at	CD24a antigen /// predicted gene, EG621324	Cd24a /// EG621	0.28	
1435407_at	---	---	0.28	
1448558_a_at	phospholipase A2, group IVA (cytosolic, calcium-dependent)	Pla2g4a	0.28	
1449319_at	R-spondin homolog (Xenopus laevis)	Rspo1	0.27	0.0487
1450757_at	cadherin 11	Cdh11	0.27	0.0132
1418243_at	ficolin A	Fcna	0.27	0.0169
1427038_at	preproenkephalin 1	Penk1	0.27	
1454974_at	similar to Netrin-1 precursor /// netrin 1	LOC672215 /// N	0.27	
1415939_at	fibromodulin	Fmod	0.26	
1418488_s_at	receptor-interacting serine-threonine kinase 4	Ripk4	0.26	
1423952_a_at	keratin 7	Krt7	0.25	
1435648_at	leucine rich repeat neuronal 4	Lrrn4	0.25	0.0046
1416832_at	solute carrier family 39 (metal ion transporter), member 8	Slc39a8	0.24	
1448377_at	secretory leukocyte peptidase inhibitor	Slpi	0.24	
1416051_at	complement component 2 (within H-2S)	C2	0.24	0.0113
1426442_at	glycoprotein m6a	Gpm6a	0.24	0.0253
1460732_a_at	periplakin	Ppl	0.24	
1449880_s_at	bone gamma-carboxyglutamate protein, related sequence 1 /// b	Bglap-rs1 /// Bgl	0.24	
1435678_at	RIKEN cDNA 2610017109 gene	2610017109Rik	0.23	
1456741_s_at	glycoprotein m6a	Gpm6a	0.21	0.0270
1449824_at	proteoglycan 4 (megakaryocyte stimulating factor, articular super	Prg4	0.21	
1451983_at	Iroquois related homeobox 1 (Drosophila)	Irx1	0.21	
1420447_at	sulfotransferase family 1E, member 1	Sult1e1	0.19	
1435026_at	sparc/osteonectin, cwcv and kazal-like domains proteoglycan 2	Spock2	0.19	
1424890_at	basonuclin 1	Bnc1	0.19	0.0154
1418301_at	interferon regulatory factor 6	Irf6	0.19	
1435831_at	uroplakin 1B	Upk1b	0.19	
1438841_s_at	arginase type II	Arg2	0.19	
1418697_at	indolethylamine N-methyltransferase	Inmt	0.19	
1455869_at	---	---	0.18	0.0161
1455464_x_at	uroplakin 1B	Upk1b	0.18	0.0245
1425471_x_at	---	---	0.17	

Online Table II

Probe Set ID	Gene Title	Gene Symbol	median of ratio	P-value
			(Ldlr <sup>-/-</sup> ) vs (Ldlr <sup>-/-</sup> Mif <sup>-/-</sup> )	
1425470_at	---	---	0.15	
1449091_at	claudin 8	Cldn8	0.15	
1419738_a_at	tropomyosin 2, beta	Tpm2	0.15	
1454881_s_at	uroplakin 3B	Upk3b	0.15	0.0321
1449178_at	PDZ and LIM domain 3	Pdlim3	0.15	
1434237_at	uroplakin 3B	Upk3b	0.14	0.0323
1448886_at	GATA binding protein 3	Gata3	0.14	
1418847_at	arginase type II	Arg2	0.13	
1417917_at	calponin 1	Cnn1	0.12	
1453085_at	serine (or cysteine) peptidase inhibitor, clade A, member 1f	Serpina1f	0.11	
1425028_a_at	tropomyosin 2, beta	Tpm2	0.10	
1452473_at	proline rich 15	Prr15	0.10	
1451335_at	placenta-specific 8	Plac8	0.09	
1449031_at	Cbp/p300-interacting transactivator with Glu/Asp-rich carboxy-terminal domain 1	Cited1	0.06	
1418207_at	FXD domain-containing ion transport regulator 4	Fxyd4	0.05	
1417156_at	keratin 19	Krt19	0.05	
1422340_a_at	actin, gamma 2, smooth muscle, enteric	Actg2	0.04	